Distributed Parameter Approach to the Dynamics of Complex Biological Processes

T. T. Lee, F. Y. Wang, and R. B. Newell
Computer-Aided Process Engineering (CAPE) Centre, Dept. of Chemical Engineering,
The University of Queensland, Brisbane 4072, Australia

Modeling and simulation of a complex biological process for the removal of nutrients (nitrogen and phosphorus) from municipal wastewater are addressed. The model developed in this work employs a distributed-parameter approach to describe the behavior of components within three different bioreaction zones and the behavior of sludge in a secondary settler. Results from a comprehensive experimental validation on an existing pilot-scale biological-nutrient-removal activated-sludge plant show that model prediction of the components' dynamics is generally good with the exception of acetate in the anaerobic zone and soluble phosphate in the aerobic zone in two experiments. Good results are achieved despite the apparent plant–model mismatch, such as uncertainties with the behavior of phosphorus-accumulating organisms. Validation of the proposed secondary-settler model shows that it is superior to two state-of-the-art models in terms of the sum of the square relative errors.

Introduction

The conventional activated-sludge plant typically consisting of, among others, a series of long-channeled bioreactors and a secondary settler has traditionally been employed for the oxidation of carbonaceous materials to carbon dioxide, biomass, and water. During the recent decades, it has been extended to allow nutrients (nitrogen and phosphorus) removal. Under the mounting pressure of problems caused by eutrophication, design, and construction of full-scale biological-nutrient-removal (BNR) activated-sludge plants have moved ahead, despite the lack of mechanistic understanding of the process, in particular biological phosphorus removal and the lack of related scientific research (Henze et al., 1987).

Evidently, mathematical models, in conjunction with prototype models such as pilot plants, are important not only for optimizing design but also for improving operation and control of these complex biological processes. Much of the work done on BNR-activated-sludge bioreactor modeling in recent years has been largely concentrated on improving the understanding of the kinetics of the process (Sen and Randall, 1992; Henze et al., 1994; Ante et al., 1994; Johannsson, 1994; Smolders et al., 1995; Barker and Dold, 1997a). The hydraulics of bioreactors, on the other hand, has often been overlooked and, although its importance has been highlighted by the mathematical modeling task group on the activated-sludge process of The International Association on Water Quality (IAWQ) (Henze et al., 1987) and recently by Barker and Dold (1997b), very little work has been done until now. Recently, a distributed parameter approach to the hydraulics of channel-type, continuous bioreactors has been addressed by the authors (Lee et al., 1999a) in a study on the dynamics of carbonaceous substrates, dissolved oxygen, and biomass within a conventional activated-sludge process. Using pilot-scale experimental data, it has been shown that this approach is superior to the widely used tanks-in-series technique, and the transient properties of three components can be correctly predicted by simulation. Lee et al. (1999b) further pointed out that their advanced hydraulics could be extended to model the BNR-activated-sludge bioreactor.

In contrast to the activated-sludge bioreactors, dynamic modeling of the activated-sludge secondary settler has received much less attention, and therefore settler models have not been fully developed. Also, there is a deficiency of model validation at full scale (Olsson and Newell, 1999). State-of-

Correspondence concerning this article should be addressed to F. Y. Wang.
Present address for T. T. Lee: Institute of High Performance Computing, 89B Science Park Drive, #01-05/08 The Rutherford, Singapore 118261.

the-art settler models for predicting the outlet sludge concentrations have been based on the solids flux theory of Coe and Clevenger (1916), which stated that total solids flux equals the sum of solids flux due to gravity settling and bulk downward movement of liquid. Based on Kynch's (1952) hypothesis on settling velocity of sludge particles, Vesilind (1968) proposed his well-known single-exponential, empirical settling velocity equation to calculate the gravity-settling flux.

Using a constrained gravity solids flux formulation and Vesilind's settling velocity equation, Vitasovic (1989) developed a distributed-parameter model to predict the profiles of sludge with respect to settler's height by assuming that the settler consists of a preselected number of equally sized layers. This so-called "layered" settler model has since become the state-of-the-art technique used by subsequent workers. Takacs et al. (1991) extended Vitasovic's work by modifying Vesilind's settling-velocity equation to a double-exponential version to account for the different behavior of small-size particles (0.5 to 5 μm) and large flocs (10 to 5,000 μm), such that the solids settling velocity decreases as concentration approaches. They further showed that their 10-layer settler model gave good predictions of effluent suspended solids, as well as excellent matches of the solids concentration profiles with respect to the length of the settler. Simple flow and concentration step tests showed that their model is able to give reasonable prediction of effluent suspended solids dynamics.

Rather than constraining the gravity solids flux, Hamilton et al. (1992) employed a model that includes a constant-dispersion term and Vesilind's gravity-settling velocity to obtain their solids concentration profiles. An independent evaluation of settler dynamic models by Grijspeerdt et al. (1995) showed that a model that incorporates Takacs et al.'s (1991) settling velocity gave the most reliable results followed by the model of Hamilton (1992), but the former requires much more computation time than the latter and more parameters to be evaluated [five parameters for Takacs et al. (1991) against three parameters for Hamilton et al. (1992)]. However, another independent evaluation of settler dynamic models carried out by Koehne et al. (1995) showed that, under different dynamic conditions, simulations with models that incorporate the settling velocities of Vesilind (1968), Takacs et al. (1991), Hartel and Popel (1992), and Otterpohl and Freund (1992) failed to give consistent results when compared to their pilot-scale experimental data. Further research is therefore needed to ascertain if other fundamental issues have been overlooked in the existing settler models.

The objectives of this work are listed as follow:

- Formulation of three different distributed-parameter bioreactor models for the BNR-activated-sludge process based on the advanced hydraulics developed in our previous work (Lee et al., 1999a,b). A modified, reduced-order activated-sludge kinetic model for biological removal of nitrogen and phosphorus, the Activated Sludge Model No. 2 (ASM No. 2) recently developed by Henze et al. (1994) is also included in the model formulation.
- Proposal for a one-dimensional, activated-sludge secondary-settler model similar to the work of Hamilton et al. (1992), but considers back mixing of upward and downward movement of the activated sludge.
- Validation of the settler model using the experimental data published by Pflanz (1969) and provides quantitative comparison with the model of Hamilton et al. (1992) and Takacs et al. (1991). This is followed by selection of an appropriate number of layers, based on a numerical investigation of the dynamics of the activated sludge.
- Development of a numerical algorithm to simulate the BNR-activated-sludge process using the distributed bioreactor models and the proposed secondary-settler model.
- Experimental validation of the distributed parameter bioreactor models using a total of nine sets of pseudo-steady-state and dynamic experimental data independently acquired from an existing BNR-activated-sludge pilot plant. Model parameters such as those related to the kinetics of biological nitrogen and phosphorus will be checked for their sensitivities toward steady-state simulation results. Concurrently, key parameters will be identified and estimated using the basis data sets. Dynamic simulation will then be performed and predicted results will be compared with plant data before concluding.

Results from this work are aimed at not only giving important insights into this challenging biological process but also providing an easy-to-implement computational algorithm for advanced control studies and design assistance both to the researchers and practitioners.

Process Description

Typically, a main-stream biological phosphorus removal process such as the *Johannesburg* configuration shown in Figure 1 consists of anaerobic, anoxic, and aerobic zones and a secondary settler with multiple recycle streams. To ensure that plug flow conditions prevail in the bioreactors, the basins are normally partitioned such that back mixing is minimized. In the anaerobic zone, fermentable organic from the influent wastewater are mixed with the return activated sludge (RAS) and converted to volatile fatty acids (VFA) by heterotrophic organisms. The latter are consumed by phosphorus accumulating organisms (PAO) and stored internally as poly-β hydroxy alkanoates (PHA). Concurrently, poly-phosphate and hence energy for VFA accumulation are released.

There is a net reduction of alkalinity and hence pH in this zone due to acids production. If the amount of VFA is insufficient, additional acids from an external source can be added to maintain a maximum PHA uptake by the biological phosphate organisms in the system. Frequently a prefermenter or an "activated" primary sedimentation tank is used to produce VFA by fermentation of readily biodegradable substrate in the incoming sewage. In the anoxic zone, nitrate (S_{NO_3}), which is recycled from the aerobic zone, is converted to dinitrogen by facultative *heterotrophic* organisms. Denitrification results in the release of alkalinity and hence an increase in pH. There is also evidence of a pronounced removal of phosphorus in this zone.

On reaching the aerobic zone, virtually all the readily biodegradable organic [hereafter referred to as biodegradable chemical oxygen demand (COD)] in the partially treated wastewater has been consumed by the heterotrophic organisms in the previous zones. In this zone, two major processes occur. In the presence of dissolved oxygen (S_{O_2}), the released

phosphate is taken up by PAO growing on the stored PHA. The phosphorus is stored internally as poly-phosphate. This results in a net reduction in phosphate in the wastewater. The second process occurring in this zone is nitrification of ammonia (S_{NH_4}) to nitrate in the wastewater by the autotrophic organisms. In order to minimize the amount of dissolved oxygen going into the anoxic zone, the last compartment is typically not aerated. Part of the sludge, which contains phosphorus to be removed, is wasted, while the remainder is returned to the anaerobic zone after thickening in the settler and additional denitrification in the RAS tank.

Model Development Based on Distributed Parameter Approach

Models for the BNR-activated-sludge bioreactors

Hydraulics and Mass Balance of the BNR-Activated-Sludge Bioreactor. The tanks-in-series technique has been widely applied to model bioreactor hydraulics, not only because of the simplicity of mathematical manipulation of a lumped-parameter system (LPS) but also because it often results in a reasonably accurate characterization of the flow pattern. Lee et al. (1999a) recently showed that the activated-sludge process dynamics can be more accurately modeled using the classic plug flow with axial dispersion technique, a distributed parameter system (DPS) approach, with reduced plant–model mismatch compared to the LPS approach. At low nutrient concentration, accuracies of hydraulic modeling become critically important, especially if the model is to be used for real-time applications. The DPS approach is therefore the preferred alternative for modeling of the main bireactors within the BNR-activated-sludge process in this work.

The general mass-balance equation for a component C_k [mgL^{-1}] within the compartmentalized anaerobic, anoxic, or aerobic zones is given by

$$\frac{\partial C_k}{\partial t} = \frac{1}{HRT} \cdot \left(\frac{1}{Pe} \frac{\partial^2 C_k}{\partial z^2} - \frac{\partial C_k}{\partial z} \right) + \sum_{p=1}^{NP} \upsilon_{p,k}\, \rho_p + M_k, \qquad (1)$$

where $\upsilon_{p,k}$ is the stoichiometric coefficient for component k and process p; ρ_p (mg L^{-1} h^{-1}) is the rate equation for process p; NP is the number of processes; M is the external mass transfer (mg L^{-1} h^{-1}); Pe is the Peclet number for a bioreaction zone; and HRT (h) is the hydraulic retention time of the zone.

The specific component mass balances at each zone can then be formulated based on Eq. 1 and the kinetic models given in the Appendix. Equations 2 to 4 show the examples of mass balances for S_A, S_{NO_3}, and S_{O_2} within the anaerobic, anoxic, and aerobic zones, respectively. Definitions of the variables and parameters for these equations can be found in Table 1.

$$\frac{\partial S_A}{\partial t} = \frac{1}{HRT} \cdot \left(\frac{1}{Pe} \frac{\partial^2 S_A}{\partial z^2} - \frac{\partial S_A}{\partial z} \right) + r_{ferm} - r_{PHA} + b_{PHA} \frac{S_{ALK}}{K_{ALK,pa} + S_{ALK}} X_{PHA}, \qquad (2)$$

where

$$r_{ferm} = q_{fe} \frac{S_F}{K_{fe} + S_F} \frac{S_{ALK}}{K_{ALK,he} + S_{ALK}} X_{PAO}$$

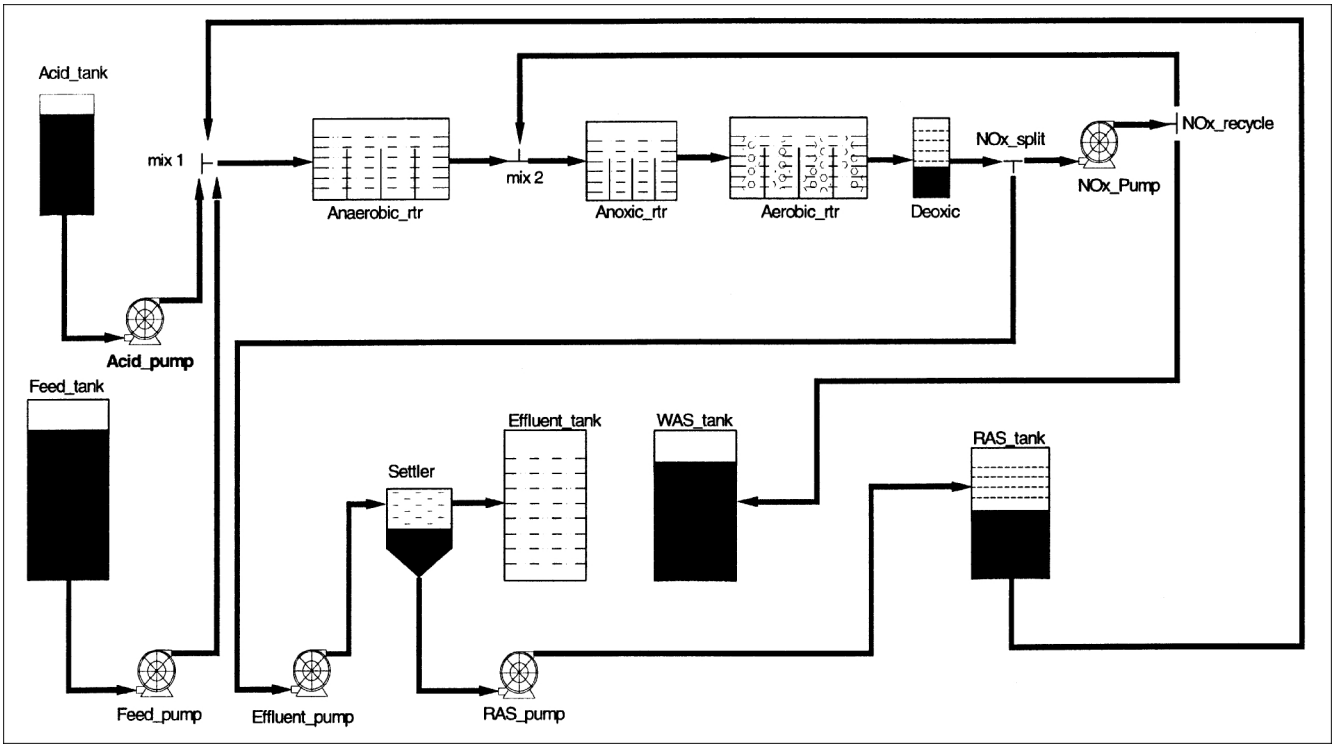

Figure 1. Typical BNR-activated-sludge process scheme.

and

$$r_{\mathrm{PHA}} = q_{\mathrm{PHA}} \frac{S_{\mathrm{A}}}{K_{\mathrm{A},pa} + S_{\mathrm{A}}} \frac{S_{\mathrm{ALK}}}{K_{\mathrm{ALK},pa} + S_{\mathrm{ALK}}} \times \frac{X_{\mathrm{PP}}/X_{\mathrm{PAO}}}{K_{\mathrm{PP}} + X_{\mathrm{PP}}/X_{\mathrm{PAO}}} X_{\mathrm{PAO}}.$$

$$\frac{\partial S_{\mathrm{NO_3}}}{\partial t} = \frac{1}{HRT} \cdot \left(\frac{1}{Pe} \frac{\partial^2 S_{\mathrm{NO_3}}}{\partial z^2} - \frac{\partial S_{\mathrm{NO_3}}}{\partial z} \right) - \frac{(1 - Y_{\mathrm{H}})}{2.86 Y_{\mathrm{H}}} (\mu_{\mathrm{H,anox\_}S_{\mathrm{F}}} + \mu_{\mathrm{H,anox\_}S_{\mathrm{A}}}) - r_{\mathrm{pp,store}} - \frac{(1 - Y_{\mathrm{PAO}})}{2.86 Y_{\mathrm{PAO}}} \mu_{\mathrm{PAO}}, \quad (3)$$

where

$$\mu_{\mathrm{H,anox\_}S_{\mathrm{F}}} = \hat{\mu}_{\mathrm{H}} \eta_{\mathrm{NO_3},he} \frac{S_{\mathrm{F}}}{K_{\mathrm{F}} + S_{\mathrm{F}}} \frac{S_{\mathrm{F}}}{S_{\mathrm{F}} + S_{\mathrm{A}}} \frac{S_{\mathrm{NH_4}}}{K_{\mathrm{NH_4},he} + S_{\mathrm{NH_4}}} \times \frac{S_{\mathrm{NO_3}}}{K_{\mathrm{NO_3},he} + S_{\mathrm{NO_3}}} \frac{S_{\mathrm{PO_4}}}{K_{\mathrm{P},he} + S_{\mathrm{PO_4}}} X_{\mathrm{H}}$$

$$\mu_{\mathrm{H,anox\_}S_{\mathrm{A}}} = \hat{\mu}_{\mathrm{H}} \eta_{\mathrm{NO_3},he} \frac{S_{\mathrm{A}}}{K_{\mathrm{A},he} + S_{\mathrm{A}}} \frac{S_{\mathrm{A}}}{S_{\mathrm{F}} + S_{\mathrm{A}}} \frac{S_{\mathrm{NH_4}}}{K_{\mathrm{NH_4},he} + S_{\mathrm{NH_4}}} \times \frac{S_{\mathrm{NO_3}}}{K_{\mathrm{NO_3},he} + S_{\mathrm{NO_3}}} \frac{S_{\mathrm{PO_4}}}{K_{\mathrm{P},he} + S_{\mathrm{PO_4}}} X_{\mathrm{H}}$$

$$r_{\mathrm{pp,store}} = \frac{Y_{\mathrm{PHA}}}{2.86} q_{\mathrm{DNP}} \frac{S_{\mathrm{PO_4}}}{K_{\mathrm{P,pp}} + S_{\mathrm{PO_4}}} \frac{X_{\mathrm{PHA}}/X_{\mathrm{PAO}}}{X_{\mathrm{PHA}} + X_{\mathrm{PHA}}/X_{\mathrm{PAO}}} \times \frac{K_{\mathrm{MAX}} - X_{\mathrm{PP}}/X_{\mathrm{PAO}}}{K_{\mathrm{IPP}} + K_{\mathrm{MAX}} - X_{\mathrm{PP}}/X_{\mathrm{PAO}}} X_{\mathrm{PAO}}$$

$$\mu_{\mathrm{PAO}} = \hat{\mu}_{\mathrm{PAO}} \frac{S_{\mathrm{NO_3}}}{K_{\mathrm{NO_3},pa} + S_{\mathrm{NO_3}}} \frac{S_{\mathrm{NH_4}}}{K_{\mathrm{NH_4},pa} + S_{\mathrm{NH_4}}} \times \frac{S_{\mathrm{PO_4}}}{K_{\mathrm{P},pa} + S_{\mathrm{PO_4}}} \frac{S_{\mathrm{ALK}}}{K_{\mathrm{ALK},pa} + S_{\mathrm{ALK}}} \frac{X_{\mathrm{PHA}}/X_{\mathrm{PAO}}}{X_{\mathrm{PHA}} + X_{\mathrm{PHA}}/X_{\mathrm{PAO}}} X_{\mathrm{PAO}}.$$

$$\frac{\partial S_{\mathrm{O_2}}}{\partial t} = \frac{1}{HRT} \cdot \left(\frac{1}{Pe} \frac{\partial^2 S_{\mathrm{O_2}}}{\partial z^2} - \frac{\partial S_{\mathrm{O_2}}}{\partial z} \right) - \left(1 - \frac{1}{Y_{\mathrm{H}}} \right) \times (\mu_{\mathrm{H},ae\_S_{\mathrm{F}}} + \mu_{\mathrm{H},ae\_S_{\mathrm{A}}}) - r_{\mathrm{PHA,store}} + \left(1 - \frac{1}{Y_{\mathrm{PAO}}} \right) \mu_{\mathrm{PAO},ae} + \left(1 - \frac{4.57}{Y_{\mathrm{AUT}}} \right) \mu_{\mathrm{AUT}} + Kla(S_{\mathrm{O_2\_SAT}} - S_{\mathrm{O_2}}) \quad (4)$$

Table 1. Notation and Typical Values of Parameters for Biological Nitrogen and Phosphorus Removal Based on Henze et al. (1994)

Parameter	Value	Units
Hydrolysis		
1. K_h = hydrolysis rate constant	0.125	h^{-1}
2. $\eta_{NO_3\_hy}$ = anoxic hydrolysis reduction factor	0.6	—
3. η_{fe} = anaerobic hydrolysis reduction factor	0.1	—
4. $K_{O_2\_hy}$ = saturation/inhibition coef. for oxygen	0.2	$g_{O_2}\ m^{-3}$
5. $K_{NO_3\_hy}$ = saturation/inhibition coef. for nitrate	0.5	$g_N\ m^{-3}$
6. K_X = saturation coefficient for particulate COD	0.1	$g_{COD} g_{COD}^{-1}$
Heterotrophic organisms		
7. $\hat{\mu}_H$ = maximum growth rate on substrate	0.25	h^{-1}
8. q_{fe} = maximum rate for fermentation	0.125	$g_{COD} g_{COD}^{-1} h^{-1}$
9 $\eta_{NO_3\_he}$ = reduction factor for denitrification	0.8	—
10. b_H = rate constant for lysis	0.0167	h^{-1}
11. $K_{O_2\_he}$ = saturation/inhibition coef. for oxygen	0.2	$g_{O_2}\ m^{-3}$
12. K_F = saturation coefficient for growth on S_F	4	$g_{COD}\ m^{-3}$
13. K_{fe} = saturation coef. for fermentation of S_F	20	$g_{COD}\ m^{-3}$
14. K_{A_he} = saturation coefficient for S_A	4	$g_{COD}\ m^{-3}$
15. $K_{KNO_3\_he}$ = saturation/inhibition coef. for nitrate	0.5	$g_N\ m^{-3}$
16. $K_{NH_4\_he}$ = saturation coefficient for ammonium	0.05	$g_N\ m^{-3}$
17. K_{P_he} = saturation coefficient for phosphorus	0.01	$g_P\ m^{-3}$
18. K_{ALK_he} = saturation coefficient for alkalinity	0.1	$mol_{HCO_3}\ m^{-3}$
Phosphorus-accumulating organisms		
19. q_{PHA} = rate constant for storage for X_{PHA}	0.125	$g_{COD}\ g_{PAO}^{-1}\ h^{-1}$
20. q_{PP} = rate contant for storage of X_{PP}	0.0625	$g_{PP}\ g_{PAO}^{-1}\ h^{-1}$
21. q_{DNP} = rate constant for denitrifying PAO*	0.03	h^{-1}
22. μ_{PAO} = maximum growth rate	0.0417	h^{-1}
23. b_{PAO} = rate constant for lysis of X_{PAO}	0.0083	h^{-1}
24. b_{PP} = rate constant for lysis of X_{PP}	0.0083	h^{-1}
25. b_{PHA} = rate contant for lysis of X_{PHA}	0.0083	h^{-1}
26. $K_{O_2\_pa}$ = saturation coefficient for S_{O_2}	0.2	$g_{O_2}\ m^{-3}$
27. K_{A_pa} = saturation coefficient for S_A	4	$g_{COD}\ m^{-3}$

*q_{DNP}, not included in the original ASM No. 2, is typically smaller than q_{PP}, because nitrate is not as good as an electron acceptor as oxygen.

Table continued

Table 1. (Continued) Notation and Typical Values of Parameters for Biological Nitrogen and Phosphorus Removal Based on Henze et al. (1994)

Parameter	Value	Units
Phosphorus-accumulating organisms — Continued		
28. $K_{NO_3\_pa}$ = saturation/inhibition coef. for nitrate	0.5	$g_N\ m^{-3}$
29. $K_{NH_4\_pa}$ = saturation coefficient for ammonium	0.05	$g_N\ m^{-3}$
30. K_{P_pp} = saturation coef. for phosphorus in PP storage	0.2	$g_P\ m^{-3}$
31. K_{P_PAO} = saturation coef. for phosphorus in growth	0.01	$g_P\ m^{-3}$
32. K_{ALK_pa} = saturation coefficient for alkalinity	0.1	$mol_{HCO_3}\ m^{-3}$
33. K_{PP} = saturation coefficient for poly-phosphate	0.01	$g_{PP}\ g_{PAO}^{-1}$
34. K_{max} = maximum ratio of X_{PP}/X_{PAO}	0.34	$g_{PP}\ g_{PAO}^{-1}$
35. K_{IPP} = inhibition coefficient for XPP storage	0.02	$g_{PP}\ g_{PAO}^{-1}$
36. K_{PHA} = saturation coefficient for PHA	0.01	$g_{PHA}\ g_{PAO}^{-1}$
Nitrifiers		
37. $\hat{\mu}_{AUT}$ = maximum growth rate	0.0417	h^{-1}
38. b_{AUT} = decay rate	0.0062	h^{-1}
39. $K_{O_2\_au}$ = saturation coefficient for oxygen	0.5	$g_{O_2}\ m^{-3}$
40. $K_{NH_4\_au}$ = saturation coefficient for ammonium	1	$g_N\ m^{-3}$
41. K_{ALK_au} = saturation coefficient for alkalinity	0.5	$mol_{HCO_3}\ m^{-3}$
42. K_{P_au} = saturation coefficient for phosphorus	0.01	$g_P\ m^{-3}$
Conversion factors		
Nitrogen		
43. i_{NSF} = N content of soluble substrate S_F	0.03	$g_N\ g_{COD}^{-1}$
44. i_{NXI} = N content of inert particulate substrate X_I	0.03	$g_N\ g_{COD}^{-1}$
45. i_{NXS} = N content of particulate substrate X_S	0.04	$g_N g_{COD}^{-1}$
46. i_{NBM} = N content of biomass X_H, X_{PAO}, X_{AUT}	0.07	$g_N g_{COD}^{-1}$
Phosphorus		
47. i_{PSF} = P content of soluble substrate S_F	0.01	$g_P g_{COD}^{-1}$
48. i_{PXS} = P content of particulate substrate X_S	0.01	$g_P g_{COD}^{-1}$
49. i_{PBM} = P content of biomass X_H, X_{PAO}, X_{AUT}	0.02	$g_P g_{COD}^{-1}$
Stoichiometric constants		
Heterotrophic organisms X_H		
50. Y_H = yield coefficient	0.63	$g_{COD} g_{COD}^{-1}$
51. f_{XI} = fraction of inert COD generated in biomass lysis	0.1	$g_{COD} g_{COD}^{-1}$
Phosphorus-accumulating organisms X_{PAO}		
52. Y_{PAO} = yield coefficient	0.63	$g_{COD} g_{COD}^{-1}$
53. Y_{PO_4} = PP requirement (S_{PO_4} release) for PHA storage	0.4	$g_{COD} g_{COD}^{-1}$
54. Y_{PHA} = PHA requirement for PP storage	0.2	$g_{COD} g_{COD}^{-1}$
55. f_{XI} = Fraction of inert COD generated in biomass lysis	0.1	$g_{COD} g_{COD}^{-1}$
Nitrifying organisms X_{AUT}		
56. Y_{AUT} = yield coefficient	0.24	$g_{COD} g_N^{-1}$
57. f_{XI} = fraction of inert COD generated in biomass lysis	0.1	$g_{COD} g_{COD}^{-1}$

*q_{DNP}, not included in the original ASM No. 2, is typically smaller than q_{PP}, because nitrate is not as good as an electron acceptor as oxygen.

where

$$\mu_{H,ae\_S_F} = \hat{\mu}_H \frac{S_{O_2}}{K_{O_2,he} + S_{O_2}} \frac{S_F}{K_F + S_F} \times \frac{S_F}{S_F + S_A} \frac{S_{NH_4}}{K_{NH_4,he} + S_{NH_4}} \frac{S_{PO_4}}{K_{P,he} + S_{PO_4}} \frac{S_{ALK}}{K_{ALK,he} + S_{ALK}} X_H$$

$$\mu_{H,ae\_S_A} = \hat{\mu}_H \frac{S_{O_2}}{K_{O_2,he} + S_{O_2}} \frac{S_A}{K_{A,he} + S_A} \frac{S_A}{S_F + S_A} \times \frac{S_{NH_4}}{K_{NH_4,he} + S_{NH_4}} \frac{S_{PO_4}}{K_{P,he} + S_{PO_4}} X_H$$

$$\mu_{PAO,ae} = \hat{\mu}_{PAO} \frac{S_{O_2}}{K_{O_2,pa} + S_{O_2}} \frac{S_{NH_4}}{K_{NH_4,pa} + S_{NH_4}} \frac{S_{PO_4}}{K_{P,pa} + S_{PO_4}} \times \frac{S_{ALK}}{K_{ALK,pa} + S_{ALK}} \frac{X_{PHA}/X_{PAO}}{X_{PHA} + X_{PHA}/X_{PAO}} X_{PAO}$$

$$\mu_{AUT} = \hat{\mu}_{AUT} \frac{S_{O_2}}{K_{O_2,au} + S_{O_2}} \frac{S_{NH_4}}{K_{NH_4,au} + S_{NH_4}} \frac{S_{PO_4}}{K_{P,au} + S_{PO_4}} \times \frac{S_{ALK}}{K_{ALK,au} + S_{ALK}} X_{AUT}$$

$$r_{PHA,store} = -Y_{PHA} q_{PP} \frac{S_{O_2}}{K_{O_2,pa} + S_{O_2}} \frac{S_{PO_4}}{K_{P,pp} + S_{PO_4}} \times \frac{X_{PHA}/X_{PAO}}{K_{PHA} + X_{PHA}/X_{PAO}} \frac{K_{max} - X_{PP}/X_{PAO}}{K_{IPP} + K_{max} - X_{PP}/X_{PAO}} X_{PAO}.$$

For a given zone, an identical Peclet number has been assumed for all the components investigated. Justifications for this assumption have been detailed in an earlier publication (Lee et al., 1999a). Equations 2 to 4 can be solved with the classic Danckwerts boundary conditions (Danckwerts, 1953). If the compartmentalized BNR-activated-sludge bioreactors

exhibited very little back mixing or "near-plug flow" conditions (such as characterized by Peclet numbers of above 20), the time-dependent exit boundary conditions described by Lee et al. (1998) could alternatively be used to circumvent numerical problems. In this work, the orthogonal collocation technique described by Villadsen and Michelsen (1978) is used to descretize the bioreactor models. The numerical solutions to Eqs. 1 to 4 and the discretized Danckwerts boundary conditions can be found in the Appendix.

Bioreaction Kinetics in the BNR-Activated-Sludge Processes. While the validity of the available kinetic models for the BNR-activated-sludge processes is yet to be fully confirmed, in particular due to the lack of experience with PAO, the ASM No. 2 was used as a basis of our study, since much of the previous work was done by the same workers. In this work, we modified the original model to "submodels" representing the three different bioreaction zones, based on a prior knowledge about the process under investigation. Matrices representing the reduced-order kinetic models of the ASM No. 2 for anaerobic, anoxic, and aerobic zones can be found in Tables 2 to 4, respectively. Notation for Tables 2 to 4 and typical values of parameters from the literature (Henze et al., 1994) can be found in Table 1.

Within the anaerobic zone, the amount of S_{O_2} is negligible or not expected to be present at all since it is not usually carried with the streams entering this zone and therefore assumed zero in the model. The influent wastewater to be treated does not usually contain S_{NO_3} since this component is a product of S_{NH_4} converted in the presence of S_{O_2} within the aerobic zone. It is possible that some S_{NO_3} may entrain to this zone from recycled sludge, but based on our pilot-plant experience, the amount is insignificant. For a properly operated plant, the S_{NO_3} should be fully denitrified once the returned sludge is pumped out of the RAS tank. In fact, S_{NO_3} in this zone must be kept at a very low concentration, typically less than 2 mg N/L since it competes with the PAO for VFA, assumed to be acetate (S_A) in the models, and hence impedes growth of the latter. Within the anoxic zone, the only source of S_{O_2} is from the oxidized nitrogen (S_{NO_x}) recycle flow. Since the last compartment of the aerobic zone in the pilot plant is not oxidized, S_{O_2} concentration typically drops to zero or close to zero in the reactor outlet and hence is neglected in the model.

In the BNR-activated-sludge process that is under study, chemicals for precipitation of phosphorus were not used and hence not considered. Soluble and particulate inert, which do not take part in the bioreaction, were removed from the original model. Total suspended solid is essentially the summation of all particulate components and is therefore removed. The final reduced-order models of the ASM No. 2 as exemplified in Tables 2 to 4 consist of 8 processes and 11 components for the anaerobic reactor, 11 processes and 12 components for the anoxic reactor, and 12 processes and 13 components for the anaerobic reactor.

While conflicting evidence concerning the fate of nitrate in biological phosphorus removal processes exists in the literature, experience at the continuous pilot-scale BNR-activated-sludge plant at the Liverpool Sewerage Treatment plant in Sydney, Australia, indicates that there has been a consistent net reduction of nitrate and phosphorus in the anoxic zone. This finding is in good agreement with a number of workers, recently reviewed by Barker and Dold (1996). The results of a recent laboratory-scale experimental study on denitrifying PAO by Wachtmeister et al. (1997) suggested that some PAO can use nitrate as an electron acceptor in the absence of oxygen for oxidation of stored poly-β hydroxy butyrate (PHB) and poly-β hydroxy valerate (PHV) and simultaneous uptake of phosphorus. These two products will hereafter be referred to by their functional group name, poly-β hydroxy alkanoates (PHA). One particular stoichiometric equation, which summarizes the essential reactions under this condition, is given by

Table 2. Reduced-Order Kinetic Model of ASM No. 2 for Anaerobic Zone

Component ⇒ Process ⇓	S_{NH_4}	S_{ALK}	S_A	S_F	S_{PO_4}	X_{AUT}	X_H	X_S	X_{PAO}	X_{PHA}	X_{PP}	Rate Equation
1. Anaerobic hydrolysis	$i_{NXS}-i_{NSF}$	$v_{1,SALK}$	0	1	$i_{PXS}-i_{PSF}$	0	0	-1	0	0	0	$K_h\eta_{fe}\dfrac{X_S/X_H}{K_x+X_S/X_H}X_H$
2. Fermentation	i_{PSF}	$v_{2,SALK}$	1	-1	i_{PSF}	0	0	0	0	0	0	$q_{fe}\dfrac{S_f}{K_{fe}+S_f}\dfrac{S_{ALK}}{K_{ALK,he}+S_{ALK}}X_H$
3. Lysis of X_H	v_{3,SNH_4}	$v_{3,SALK}$	0	0	v_{3,SPO_4}	0	-1	$1-f_{XI}$	0	0	0	$b_H X_H$
4. Stor of X_{PHA}	0	$v_{4,SALK}$	-1	0	Y_{PO_4}	0	0	0	0	1	$-Y_{PO_4}$	$q_{PHA}\dfrac{S_A}{K_{A,pa}+S_A}\dfrac{S_{ALK}}{K_{ALK,pa}+S_{ALK}}\times\dfrac{X_{PP}/X_{PAO}}{K_{PP}+X_{PP}/X_{PAO}}X_{PAO}$
5. Lysis of X_{PAO}	v_{5,SNH_4}	$v_{5,SALK}$	0	0	v_{5,SPO_4}	0	0	$1-f_{XI}$	-1	0	0	$b_{PAO}X_{PAO}$
6. Lysis of X_{PP}	0	$-1.5/31$	0	0	1	0	0	0	0	0	-1	$b_{PP}X_{PP}S_{ALK}/(K_{ALK,pa}+S_{ALK})$
7. Lysis of X_{PHA}	0	$-1/64$	1	0	0	0	0	0	0	-1	0	$b_{PHA}X_{PHA}S_{ALK}/(K_{ALK,pa}+S_{ALK})$
8. Lysis of X_{AUT}	v_{8,SNH_4}	$v_{8,SALK}$	0	0	v_{8,SPO_4}	-1	0	$1-f_{XI}$	0	0	0	$b_{AUT}X_{AUT}$

NOTES: $v_{i,c}$: i = Process number; c = component.

$v_{3,SNH_4}=v_{5,SNH_4}=v_{8,SNH_4}=-(f_{XI}\times i_{NXI}+(1-f_{XI})\times i_{NXS}-i_{NBM})$

$v_{1,SALK}=v_{1,SNH_4}/14-v_{1,SPO_4}\times 1.5/31$

$v_{2,SALK}=-1/64+v_{2,SNH_4}/14-v_{2,SPO_4}\times 1.5/31$

$v_{3,SALK}=v_{3,SNH_4}/14-v_{3,SPO_4}\times 1.5/31$

$v_{4,SALK}=1/64-Y_{PO_4}\times 1.5/31$

$v_{5,SALK}=v_{5,SNH_4}/14-v_{5,SPO_4}\times 1.5/31$

$v_{8,SALK}=v_{8,SNH_4}/14-v_{8,SPO_4}\times 1.5/31$

$v_{3,SPO_4}=v_{5,SPO_4}=v_{8,SPO_4}=-(f_{XI}\times i_{PXI}+(1-f_{XI})\times i_{PXS}-i_{PBM})$

Table 3. Reduced-Order Kinetic Model of ASM No. 2 For Anoxic Zone

Component ⇒ Process ⇓	S_{NO_3}	S_{NH_4}	S_{ALK}	S_A	S_F	S_{PO_4}	X_{AUT}	X_H	X_S	X_{PAO}	X_{PHA}	X_{PP}	Rate Equation
1. Anoxic hydrolysis	0	$i_{NXS}-i_{NSF}\upsilon_{1,SALK}$		0	1	$i_{PXS}-i_{PSF}$	0	0	-1	0	0	0	$K_h\eta_{NO_3,hy}\frac{S_{NO_3}}{K_{NO_3,hy}+S_{NO_3}}\times\frac{X_S/X_H}{K_x+X_S/X_H}X_H$
2. Anoxic growth of X_H on S_F	$\frac{-1(-Y_H)}{2.86Y_H}$	$\frac{i_{NSF}}{Y_H}-i_{NBM}$	$\upsilon_{2,SALK}$	0	$-1/Y_H$	$\frac{i_{PSF}}{Y_H}-i_{PBM}$	0	1	0	0	0	0	$\eta_H\eta_{NO_3,ha}\frac{S_F}{K_F+S_F}\times\frac{S_F}{S_F+S_A}\frac{S_{NH_3}}{K_{NH_3,he}+S_{NH_4}}\times\frac{S_{NO_3}}{K_{NO_3,he}+S_{NO_3}}\frac{S_{PO_4}}{K_{P,he}+S_{PO_4}}X_H$
3. Anoxic growth of X_H on S_A	$\frac{-(1-Y_H)}{2.86Y_H}$	$-i_{NBM}$	$\upsilon_{3,SALK}$	$-\frac{1}{Y_H}$	0	i_{PBM}	0	1	0	0	0	0	$\hat{\mu}_H\eta_{NO_3,he}\frac{S_A}{K_{A,he}+S_A}\frac{S_A}{S_F+S_A}\times\frac{S_{NH_4}}{K_{NH_4,ha}+S_{NH_4}}\frac{S_{NO_3}}{K_{NO_3,he}+S_{NO_3}}\times\frac{S_{PO_4}}{K_{P,he}+S_{PO_4}}X_H$
4. Lysis of X_H	0	υ_{4,SNH_4}	$\upsilon_{4,SALK}$	0	0	υ_{4,SPO_4}	0	-1	$1-f_{XI}$	0	0	0	$b_H X_H$
5. Stor of X_{PHA}	0	0	$\upsilon_{5,SALK}$	-1	0	Y_{PO_4}	0	0	0	0	1	$-Y_{PO_4}$	$q_{PHA}\frac{S_A}{K_{A,pa}+S_A}\frac{S_{ALK}}{K_{ALK,pa}+S_{ALK}}\times\frac{X_{PP}/X_{PAO}}{K_{PP}+X_{PP}/X_{PAO}}X_{PAO}$
6. Stor of X_{PP}	$\frac{-Y_{PHA}}{2.86}$	0	$\upsilon_{6,SALK}$	0	0	-1	0	0	0	0	$-Y_{PHA}$	1	$q_{DNP}\frac{S_{NO_3}}{K_{NO_2,pa}+S_{NO_3}}\frac{S_{NO_3}}{K_{P,pp}+S_{PO_4}}\times\frac{X_{PHA}/X_{PAO}}{K_{PHA}+X_{PHA}/X_{PAO}}\times\frac{K_{max}-X_{PP}/X_{PAO}}{K_{PP}+K_{max}-X_{PP}/X_{PAO}}X_{PAO}$
7. Anoxic growth of X_{PAO} on X_{PHA}	$\frac{-(1-Y_{PAO})}{2.86Y_{PAO}}$	$-i_{NBM}$	$\upsilon_{7,SALK}$	0	0	$-i_{PBM}$	0	0	0	1	$-\frac{1}{Y_{PAO}}$	0	$\hat{\mu}_{PAO}\frac{S_{NO_3}}{K_{NO_3,pa}+S_{NO_3}}\frac{S_{NH_4}}{K_{NH_4,pa}+S_{NH_4}}\times\frac{S_{ALK}}{K_{ALK,pa}+S_{ALK}}\frac{S_{PO_4}}{K_{P,pa}+S_{PO_4}}\times\frac{X_{PHA}/X_{PAO}}{K_{PHA}+X_{PHA}/X_{PAO}}X_{PAO}$
8. Lysis of X_{PAO}	0	υ_{8,SNH_4}	$\upsilon_{8,SALK}$	0	0	υ_{8,SPO_4}	0	0	$1-f_{XI}$	-1	0	0	$b_{PAO}X_{PAO}$
9. Lysis of X_{PP}	0	0	$-1/31$	0	0	1	0	0	0	0	0	-1	$b_{PP}X_{PP}S_{ALK}/(K_{ALK,pa}+S_{ALK})$
10. Lysis of X_{PHA}	0	0	$-1/64$	1	0	0	0	0	0	0	-1	0	$b_{PHA}X_{PHA}S_{ALK}/(K_{ALK,pa}+S_{ALK})$
11. Lysis of X_{AUT}	0	υ_{11,SNH_4}	$\upsilon_{11,SALK}$	0	0	υ_{11,SPO_4}	-1	0	$1-f_{XI}$	0	0	0	$b_{AUT}X_{AUT}$

NOTES:
$\upsilon_{4,SNH_4}=\upsilon_{8,SNH_4}=\upsilon_{11,SNH_4}=-(f_{XI}\times i_{NXI}+(1-f_{XI})\times i_{NXS}-i_{NBM})$
$\upsilon_{1,SALK}=\upsilon_{1,SNH_4}/14-1.5\upsilon_{1,SPO_4}/31$
$\upsilon_{2,SALK}=(1-Y_H)/(2.86\,Y_H)/14+\upsilon_{2,SNH_4}/14-1.5\upsilon_{2,SPO_4}/31$
$\upsilon_{3,SALK}=1/(64\,Y_H)+(1-Y_H)/(2.86\,Y_H)/14+\upsilon_{3,SNH_4}/14-1.5\upsilon_{3,SPO_4}/31$
$\upsilon_{4,SALK}=\upsilon_{4,SNH_4}/14-1.5\upsilon_{4,SPO_4}/31$
$\upsilon_{5,SALK}=1/64-1.5\,Y_{PO_4}/31$
$\upsilon_{6,SALK}=Y_{PHA}/2.86/14+1.5/31$
$\upsilon_{7,SALK}=1.5\,i_{PBM}/31+\upsilon_{7,SNH_4}/14+(1-Y_{PAO})/(2.86\upsilon_{7,PAO})/14$
$\upsilon_{8,SALK}=\upsilon_{8,SNH_4}/14-1.5\upsilon_{8,SPO_4}/31$
$\upsilon_{11,SALK}=\upsilon_{11,SNH_4}/14-1.5\upsilon_{11,SPO_4}/31$
$\upsilon_{4,SPO_4}=\upsilon_{8,SPO_4}=\upsilon_{11,SPO_4}-(f_{XI}\times i_{PXI}+(1-f_{XI})\times i_{PXS}-i_{PBM})$

$$\underset{\text{(acetic acid)}}{C_2H_4O_2}+0.16\underset{\text{(ammonium)}}{NH_4^+}+0.2\underset{\text{(phosphate)}}{PO_4^{3-}}+0.96\underset{\text{(nitrate)}}{NO_3^-}$$

$$\downarrow$$

$$0.16\underset{\text{(biomass)}}{C_5H_7NO_2}+\underset{\text{(carbon dioxide)}}{1.2CO_2}+0.2\underset{\text{(polyphosphate)}}{(HPO_3)}+\underset{\text{(hydroxide)}}{1.4OH^-}+\underset{\text{(nitrogen)}}{0.48N_2}+\underset{\text{(water)}}{0.96H_2O}.$$

Although the fraction of the denitrifying PAO cannot be precisely ascertained for the time being, their effect in predicting the fate of species such as nitrate and phosphate within the anoxic zone could be significant. We have therefore incorporated stoichiometry and process rates for denitrifying PAO into the reduced-order ASM No. 2 (see Table 3) for the anoxic reactor; thus, the original ASM No. 2 is slightly modified.

Table 4. Reduced-Order Kinetic Model of ASM No. 2 for Aerobic Zone

Component ⇒ Process ⇓	S_{O_2}	S_{NO_3}	S_{NH_4}	S_{ALK}	S_A	S_F	S_{PO_4}	X_{AUT}	X_H	X_S	X_{PAO}	X_{PHA}	X_{PP}	Rate Equation
1. Aerobic hydrolysis	0	0	$i_{NXS}-i_{NSF}$	$v_{1,SALK}$	0	1	$i_{PXS}-i_{PSF}$	0	0	−1	0	0	0	$K_h\frac{S_{O_2}}{K_{O_2-hy}+S_{O_2}}\frac{X_S/X_H}{K_x+X_S/X_H}X_H$
2. Aerobic growth of X_H on S_F	$\frac{-(1-Y_H)}{Y_H}$	0	i_{NSF}/Y_H-i_{NBM}	$v_{2,SALK}$	0	$\frac{-1}{Y_H}$	i_{PSF}/Y_H-i_{NBM}	0	1	0	0	0	0	$\hat{\mu}_H\frac{S_{O_2}}{K_{O_2,he}+S_{O_2}}\frac{S_F}{K_F+S_F}\times\frac{S_F}{S_F+S_A}\frac{S_{NH_4}}{K_{NH_4,he}+S_{NH_4}}\times\frac{S_{PO_4}}{K_{P,he}+S_{PO_4}}\frac{S_{ALK}}{K_{ALK,he}+S_{ALK}}X_H$
3. Aerobic growth of X_H on S_A	$\frac{-(1-Y_H)}{Y_H}$	0	$-i_{NBM}$	$v_{3,SALK}$	$\frac{-1}{Y_H}$	0	$-i_{PBM}$	0	1	0	0	0	0	$\hat{\mu}_H\frac{S_{O_2}}{K_{O_2,he}+S_{O_2}}\frac{S_A}{K_{A,he}+S_A}\frac{S_A}{S_F+S_A}\times\frac{S_{NH_4}}{K_{NH_4,he}+S_{NH_4}}\frac{S_{PO_4}}{K_{P,he}+S_{PO_4}}X_H$
4. Lysis of X_H	0	0	v_{4,SNH_4}	$v_{4,SALK}$	0	0	v_{4,SPO_4}	0	−1	$1-f_{XI}$	0	0	0	$b_H X_H$
5. Stor of X_{PHA}	0	0	0	$v_{5,SALK}$	−1	0	Y_{PO_4}	0	0	0	0	1	$-Y_{PO_4}$	$q_{PHA}\frac{S_A}{K_{A,pa}+S_A}\frac{S_{ALK}}{K_{ALK,pa}+S_{ALK}}\times\frac{X_{PP}/X_{PAO}}{K_{PP}+X_{PP}/X_{PAO}}X_{PAO}$
6. Stor of X_{PP}	$-Y_{PHA}$	0	0	1.5/31	0	0	−1	0	0	0	0	$-Y_{PHA}$	1	$q_{PP}\frac{S_{O_2}}{K_{O_2,pa}+S_{O_2}}\frac{S_{PO_4}}{K_{P,pp}+S_{PO_4}}\times\frac{X_{PHA}/X_{PAO}}{K_{PHA}+X_{PHA}/X_{PAO}}\times\frac{K_{max}-X_{PP}/X_{PAO}}{K_{PP}+K_{max}-X_{PP}/X_{PAO}}X_{PAO}$
7. Aerobic growth of X_{PAO} on X_{PHA}	$\frac{-(1-Y_{PAO})}{Y_{PAO}}$	0	$-i_{NBM}$	$v_{7,SALK}$	0	0	$-i_{PBM}$	0	0	0	1	$-\frac{1}{Y_{PAO}}$	0	$\hat{\mu}_{PAO}\frac{S_{O_2}}{K_{O_2,pa}+S_{O_2}}\frac{S_{NH_4}}{K_{NH_4,pa}+S_{NH_4}}\times\frac{S_{ALK}}{K_{ALK,pa}+S_{ALK}}\frac{S_{PO_4}}{K_{P,pa}+S_{PO_4}}\times\frac{X_{PHA}/X_{PAO}}{K_{PHA}+X_{PHA}/X_{PAO}}X_{PAO}$
8. Lysis of X_{PAO}	0	0	v_{8,SNH_4}	$v_{8,SALK}$	0	0	v_{8,SPO_4}	0	0	$1-f_{XI}$	−1	0	0	$b_{PAO}X_{PAO}$
9. Lysis of X_{PP}	0	0	0	−1.5/31	0	0	1	0	0	0	0	0	−1	$b_{PP}X_{PP}S_{ALK}/(K_{ALK,pa}+S_{ALK})$
10. Lysis of X_{PHA}	0	0	0	−1/64	1	0	0	0	0	0	0	−1	0	$b_{PHA}X_{PHA}S_{ALK}/(K_{ALK,pa}+S_{ALK})$
11. Growth of X_{AUT}	$1-\frac{4.57}{Y_{AUT}}$	$\frac{1}{Y_{AUT}}$	$-i_{NBM}-\frac{1}{Y_{AUT}}$	$v_{11,SALK}$	0	0	$-i_{PBM}$	1	0	0	0	0	0	$\hat{\mu}_{AUT}\frac{S_{O_2}}{K_{O_2,au}+S_{O_2}}\frac{S_{NH_4}}{K_{NH_4,au}+S_{NH_4}}\times\frac{S_{PO_4}}{K_{P,au}+S_{PO_4}}\frac{S_{ALK}}{K_{ALK,au}+S_{ALK}}X_{AUT}$
12. Lysis of X_{AUT}	0	0	v_{12,SNH_4}	$v_{12,SALK}$	0	0	v_{12,SPO_4}	−1	0	$1-f_{XI}$	0	0	0	$b_{AUT}X_{AUT}$

Notes:
$v_{4,SNH_4}=v_{8,SNH_4}=v_{12,SNH_4}-(f_{XI}\times i_{NXI}+(1-f_{XI})\times i_{NXS}-i_{NBM})$
$v_{1,SALK}=v_{1,SNH_4}/14-v_{1,SPO_4}\times 1.5/31$
$v_{2,SALK}=v_{2,SNH_4}/14-v_{2,SPO_4}\times 1.5/31$
$v_{3,SALK}=1/64\ Y_H+v_{3,SNH_4}/14-v_{3,SPO_4}\times 1.5/31$
$v_{4,SALK}=v_{4,SNH_4}/14-v_{4,SPO_4}\times 1.5/31$
$v_{5,SALK}=1/64-Y_{PO_4}\times 1.5/31$
$v_{7,SALK}=1.5/31\times i_{PBM}+v_{7,SNH_4}/14$
$v_{8,SALK}=v_{8,SNH_4}/14-v_{8,SPO_4}\times 1.5/31$
$v_{11,SALK}=-i_{NBM}/14-2/Y_{AUT}/14+i_{PBM}\times 1.5/31$
$v_{12,SALK}=v_{11,SNH_4}/14-v_{11,SPO_4}\times 1.5/31$
$v_{4,SPO_4}=v_{8,SPO_4}=v_{12,SPO_4}=-(f_{XI}\times i_{NXI}+(1-f_{XI})\times i_{PXS}-i_{PBM})$

Models for the secondary settler

We consider that a settler can be divided into two distinct zones, namely clarification and thickening as shown in Figure 2 (top). Treated wastewater from an activated-sludge reactor typically enters the settler via a center port, usually showing a strong flocculating tendency. If a batch-settling test is performed on the same feed, one would be able to visualize that a solid−liquid interface develops immediately after settling commences. Hereafter, the low-concentration phase and the high-concentration phase are denoted as clarification and thickening zones, respectively. During thickening, three physical phenomena are observed to occur: (1) zone-settling mode,

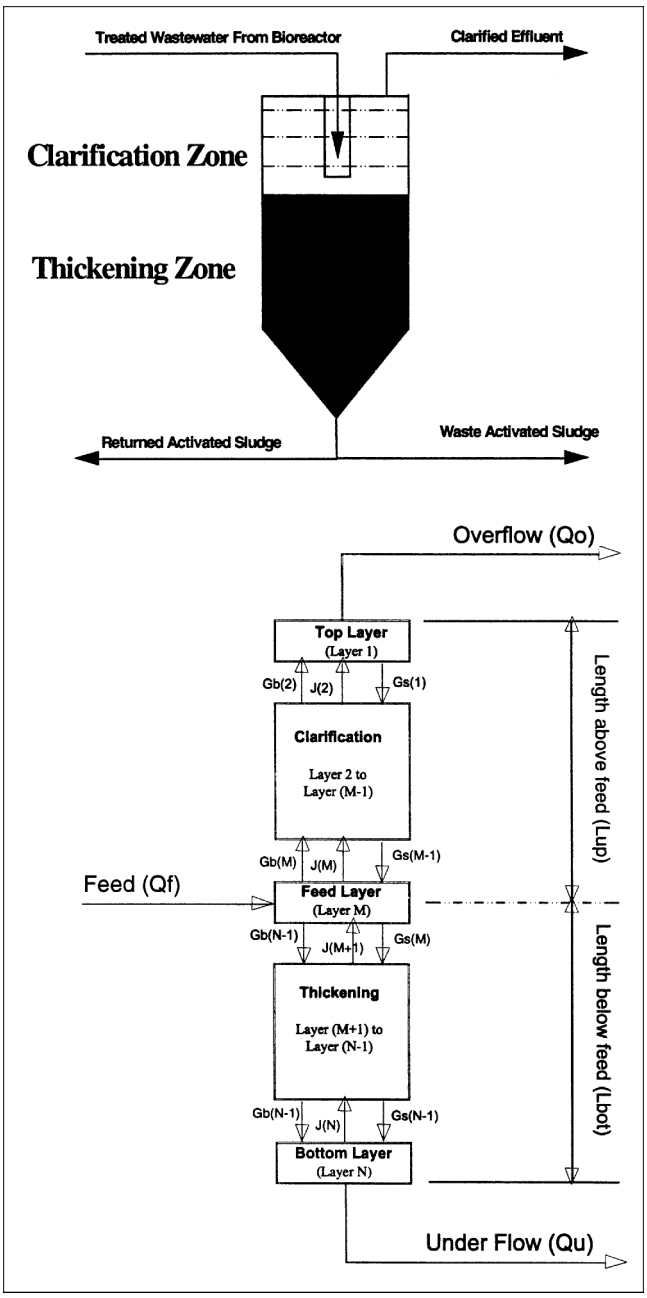

Figure 2. Secondary settler (top figure) and discretization of a settler model (bottom figure).

(2) transition stage, and (3) compression. Only the zone-settling mode, which is the governing phenomenon (WRC, 1984) will be considered in this work. This thickening behavior assumes that all particles settled at the same rate throughout the zone depth.

A model for solids dynamics within the thickening zone is given by

$$\frac{\partial X}{\partial t} = -\frac{Q_U}{A}\frac{\partial X}{\partial Z} - \frac{\partial (V_S X)}{\partial Z} + D_S \frac{\partial^2 X}{\partial Z^2}, \tag{5}$$

where Q_U is the downward volumetric flow rate; V_S is the gravity-settling velocity; and D_S is the dispersion coefficient of solids in the thickening zone. Derivation of Eq. 5 is given in the Appendix. An expression developed by Takacs et al. (1991) for the gravity-settling velocity is given by

$$V_S = \max\Big(0, \min\Big[V_{O\_}, V_O\big(e^{-r_h(X-X_{\min})} - e^{-r_p(X-X_{\min})}\big)\Big]\Big), \tag{6}$$

where V_O and r_h are the empirical settling parameters of Vesilind (1968), r_p is a settling parameter for low-concentration suspended solids; $V_{O\_}$ is maximum settling velocity; and $X_{\min}$ is minimum attainable suspended solids concentration. The parameters V_O, r_h, r_p, $V_{O\_}$, and $X_{\min}$ are regarded as constants that require estimation.

A model for solids dynamics within the clarification zone can be similarly derived and is given by Eq. 7:

$$\frac{\partial X}{\partial t} = -\frac{Q_O}{A}\frac{\partial X}{\partial Z} + \frac{\partial (V_S X)}{\partial Z} + D'_S \frac{\partial^2 X}{\partial Z^2}, \tag{7}$$

where Q_O is the upward volumetric flow rate, and D'_S is the sludge-dispersion coefficient in the clarification zone. It must be pointed out that the dispersion coefficient for the clarification and thickening zones may be different, largely depending on the settler design. It must also be pointed out that we have ignored the geometrical effects such as the conical-shaped bottom often found in practical settling tanks, but the impact is deemed insignificant (Watts et al., 1996). The settler model given by Eqs. 5 and 7 can be solved numerically by using a finite difference scheme. Figure 2 (bottom) shows the numerical division of a settler into five sections, namely: (1) top layer (that is, layer 1); (2) clarification layer [that is, layer 2 to layer (M − 1)]; (3) feed layer (that is, layer M); thickening layer [that is, layer (M + 1) to layer (N − 1)]; and (4) bottom layer (that is, layer N). A computational algorithm can now be developed, bearing in mind that all layers have an identical height of ΔZ.

Layer 1. Based on Eq. 5 and Figure 2 (bottom), a discretized mass balance for layer 1 is given by

$$\frac{dX_1}{dt} = \frac{Q_O(X_2 - X_1) - V_{S,1}X_1 A + \dfrac{Q_O L_{\text{up}}}{Pe_{\text{up}}}\left(\dfrac{X_2 - X_1}{\Delta Z}\right)}{A \cdot \Delta Z}, \tag{8}$$

where L_{up} = length of clarification zone, and $Pe_{\text{up}} = (U \cdot L_{\text{up}})/D'_S$ is the Peclet number at the clarification zone.

Layers 2 to (M − 1). Based on Eq. 5 and Figure 2 (bottom), discretized mass balances for layers 2 to (M − 1) are given by

$$\frac{dX_i}{dt} = \frac{Q_O(X_{i+1} - X_i) + V_{S,i-1}X_{i-1}A - V_{S,i}X_i A + \dfrac{Q_O L_{\text{up}}}{Pe_{\text{up}}}\left(\dfrac{X_{i+1} - 2X_i + X_{i-1}}{\Delta Z}\right)}{A \cdot \Delta Z}, \tag{9}$$

where $i = 2, \ldots, (M-1)$.

Feed Layer (layer M). Based on Eqs. 5, 7, and Figure 2 (bottom), discretized mass balance for the feed layer is given by

$$\frac{dX_M}{dt} = \frac{Q_f(X_f - X_M) + V_{S,M-1}X_{M-1}A - V_{S,M}X_M A + \dfrac{Q_O L_{up}}{Pe_{up}}\left(\dfrac{X_{M+1} - X_M}{\Delta Z}\right) - \dfrac{Q_U L_{bot}}{Pe_{bot}}\left(\dfrac{X_M - X_{M-1}}{\Delta Z}\right)}{A \cdot \Delta Z}, \tag{10}$$

where L_{bot} = length of thickening zone, and $Pe_{bot} = (U \cdot L_{bot})/D_S$ is the Peclet number at the thickening zone.

Layers (M + 1) to (N − 1). Based on Eq. 7 and Figure 2 (bottom), discretized mass balances for layers (M + 1) to (N − 1) are given by

$$\frac{dX_j}{dt} = \frac{Q_U(X_{j-1} - X_j) + V_{S,j-1}X_{j-1}A - V_{S,j}X_j A + \dfrac{Q_U L_{bot}}{Pe_{bot}}\left(\dfrac{X_{j+1} - 2X_j + X_{j-1}}{\Delta Z}\right)}{A \cdot \Delta Z}, \tag{11}$$

where $j = (M+1), \ldots, (N-1)$.

Bottom Layer (layer N). Based on Eq. 7 and Figure 2 (bottom), discretized mass balances for layers N are given by

$$\frac{dX_N}{dt} = \frac{Q_U(X_{N-1} - X_N) + V_{S,N-1}X_{N-1}A - \dfrac{Q_U L_{bot}}{Pe_{bot}}\left(\dfrac{X_N - X_{N-1}}{\Delta Z}\right)}{A \cdot \Delta Z}. \tag{12}$$

The complete mathematical representation for the discretized settler model given by Eqs. 8 to 12 is hereafter called the *double-Peclet* settler model. In summary, this proposed settler model, which differs from other models in the literature, considers back mixing or dispersion of sludge in the upward and downward directions. If back mixing within the two zones is either insignificant or close enough, we can reduce the double-Peclet settler model to a *single-Peclet* settler model by defining

$$Pe_{settler} = Pe_{up} = Pe_{bot}. \tag{13}$$

Simplified models for subordinate systems

The RAS tank and the deoxic or nonaerated compartment of the aerobic zone are assumed to be well-mixed. In that case, they are modeled using simple lumped-parameter schemes. The lumped-parameter models used in this study assume that concentration of components at the outlet of the tank equals concentration of components within the tank. The RAS tank and the unaerated compartment models used the kinetics of the anoxic zone in Table 3 and the aerobic zone in Table 4, respectively. For model simulation, inlet streams to a bioreactor are assumed to be initially mixed to obtain volume-average stream properties, although they are introduced independently into a reactor in the real plant. This is not thought to cause any problems since the streams are considered to be thoroughly mixed at the time of entering the reactor. Split streams are assumed to have identical properties as the inlet stream prior to splitting.

Validation of the Distributed-Parameter Models

Steady-state validation and dynamics of the secondary-settler models

The discretized secondary-settler model will now be applied to model the full-scale secondary settler of Pflanz (1969). Models of Takacs et al. (1991) and Hamilton et al. (1992) also will be included in this study for comparative purposes. The Peclet numbers of the proposed model can be calculated from the standard retention time distribution (RTD) experiments (Levenspiel, 1972). Since experimental data for RTD are unavailable, the only sensible way to overcome this problem is to estimate the parameters. As with studies on the same settler by previous workers (Takacs et al., 1991; Watts et al., 1996), all model parameters are estimated based on the experimental results of Pflanz (1969). In this work, the nonlinear multivariable optimization technique of Levenberg-Marquardt (Reklaitis et al., 1983) is employed to estimate the "best" parameters for each model under investigation to ensure that comparison is on a common basis. The model will then be validated against two independent sets of experimental data, which were collected by Pflanz under different operating conditions.

Pflanz's "Benchmark" Experiments. Pflanz (1969) investigated the settling properties of the activated sludge at a full-scale activated-sludge treatment plant at Celle, Federal Republic of Germany. The plant largely treated domestic sewage. The settler was a 33-m-diam., circular-built basin with a total depth of 2.27 m and an effective volume of 1800 m^3. Experiments with three different loads of 360 m^3/h, 450 m^3/h, and 600 m^3/h were conducted and samples were collected at

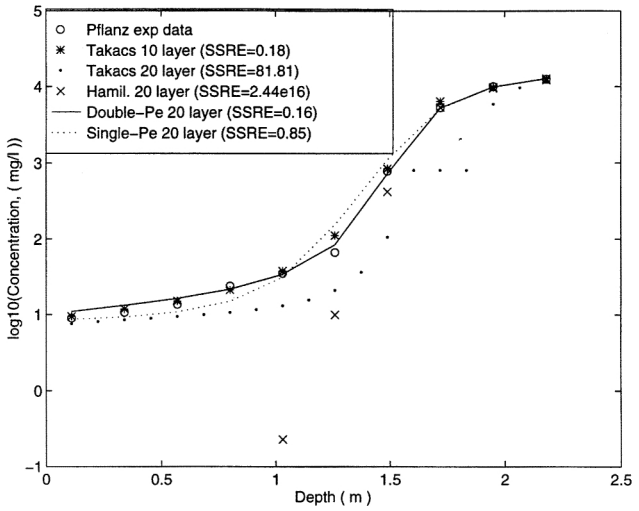

Figure 3. Steady-state sludge concentration profiles of various 1-D settler models compared with Pflanz's (1969) benchmark experimental data.

different depths of equal range along the settler's depth and at different radial points. The inlet sludge concentration was 5620 g/m^3, 5520 g/m^3, and 5100 g/m^3, respectively. Feed enters the settler at a depth of approximately 1.25 m.

Results and Discussion on Steady-State Validation of the Settler Models. Figure 3 compares the sludge concentrations obtained by using various models, namely, the proposed double-Peclet and single-Peclet models and models developed by Takacs et al. (1991) and by Hamilton et al. (1992) with Pflanz's experimental data. Feed to the settler was the low-load case of 360 m^3/h and the detention time was 5 h. The sum of square relative errors (SSRE) indicated in Figure 3 is defined as

$$\text{SSRE} = \sum_{i=1}^{N} W_i \left(\frac{X_{f,i} - X_{\text{exp},i}}{X_{\text{exp},i}} \right)^2, \qquad (14)$$

where W_i = weighting function for the ith point. In this study, an equal weighting was employed for the entire length of the settler. The parameter $X_{f,i}$ = simulated concentration, $X_{\text{exp},i}$ = experimental data, and N = number of layers.

Clearly, the 10-layer Takacs model gives an excellent fit to the experimental data with an SSRE of 0.18. Instead of giving a more accurate prediction with increased discretization, the 20-layer Takacs model failed to give reasonable predictions within the settler depth of between 1.48 and 1.93 m, which in fact was the thickening zone. This result is consistent with the findings of Jeppson and Diehl (1996) and Watts et al. (1996). The resulting SSRE was larger than the 10-layer model by more than 80 times. This anomaly was attributable to the numerical problem resulting from the formulation of their gravity settling flux. On the other hand, the single-Peclet model with 20 layers proposed in this study appears to give a reasonably good prediction of the sludge concentration profile with an SSRE of 0.85. However, the error at the feeding point, at a settler depth of 1.25 m appears to be pronounced, when the single-Peclet model is employed. This error may be attributable to the oversimplification of the back-mixing effect by the single-Peclet number term. Figure 3 also shows that the model proposed by Hamilton et al. (1992) failed to predict the sludge concentration at the clarification zone (0 to 1.5 m deep), satisfactorily resulting in an extremely large SSRE compared with other models investigated. This can be attributable to the fact that the effect of small particles was not accounted for in the single-exponential, Vesilind's settling velocity employed in their work. With an SSRE of 0.16, the proposed double-Peclet model with 20 layers gives the best result in this study.

The optimized parameters for each of the model are given in Table 5. It is interesting to note that the parameter V_O of each model falls within the pooled data from batch settling tests done by the WRC (1984) in South Africa, and the optimized parameter r_h of the double-Peclet model and the model developed by Takacs et al. (1991) are closest to their best results. Concerning the parameters in the new model, the value of Pe_{up} is evidently much higher than Pe_{bot}, thus suggesting that the amount of back mixing within the clarification zone was relatively less than the thickening zone in Pflanz's settler.

Figure 4 (top) shows simulated results using the double-Peclet model with the estimated parameters in Table 5 compared with Pflanz's medium-load experimental data. Clearly, the double-Peclet model is able to give a good prediction of the sludge profile, and the calculated SSRE was as low as 0.90. Figure 4 (bottom) compares simulated results with Pflanz's high-load experimental data. The predicted sludge profile at the thickening zone below 1.5-m depth is quite good, but the profile in the clarification zone appears to be slightly underpredicted and hence the overall prediction is not as good as the medium-load case. Nevertheless, the resulting SSRE for this case is still reasonably low, with a value of 2.37. If the high loading data rather than low loading data are optimized, fitted profile at the clarification zone is good, but the values of all new parameter estimates (Lee, 1998) are similar to the numbers shown in Table 5, thus implying that the model is extremely sensitive to the parameters.

Dynamics of the Settler. Using the 20-layer, double-Peclet model with parameters identified in Table 5, the result of

Table 5. Estimated Parameters Fitted to Pflanz's Low-Load Experimental Data

	Settler Model			
Parameter	Double-*Pe* (20-layer)	Single-*Pe* (20-Layer)	Takacs et al. (10-Layer)	Hamilton et al. (20-Layer)
V_O (m/h)	15.4036	5.9061	10.201	5.3267
V_{O-} (m/h)	7.0184	7.3065	6.3756	—
r_h (m^3/kg)	0.2773	0.3355	0.3638	0.3694
r_p (m^3/kg)	3.8616	34.3803	5.8248	—
X_{min} (g/m^3)	6.8356	8.2126	6.9126*	—
Pe_{settler}	—	3.3091	—	—
Pe_{up}	4.2205	—	—	—
Pe_{bot}	0.3731	—	—	—
f_{ns}	—	—	1.23×10^{-3}	—
D (m^2/s)	—	—	—	11.7263

*$X_{\text{min}} = X_f x_{fns}$; f_{ns} = nonsettleable solids; X_f = feed concentration = 5620 g/m^3.

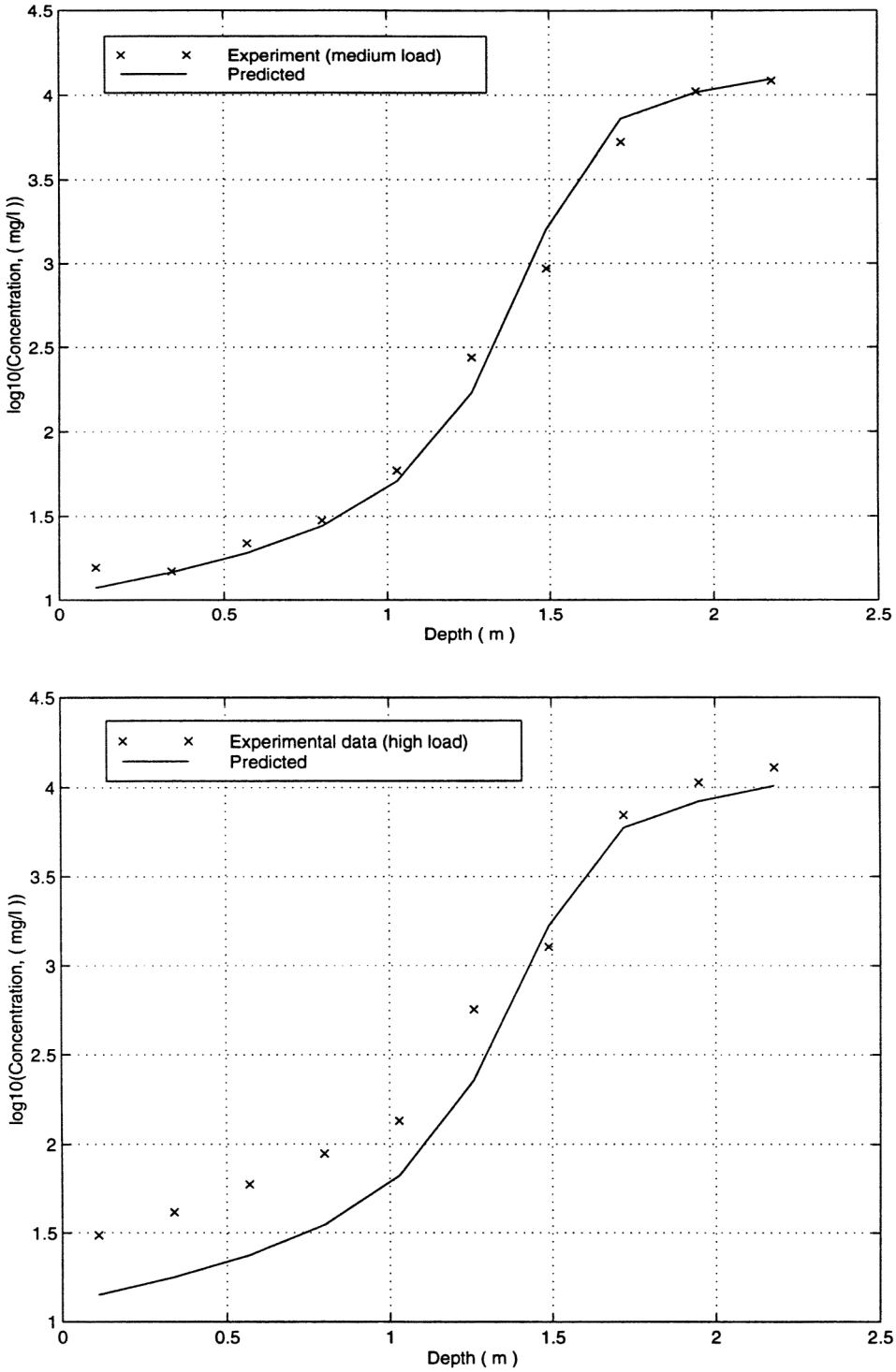

Figure 4. Prediction of sludge profile for Pflanz's medium-load case (top figure) and high-load case (bottom figure) using the double-*Pe* settler model.

simulated sludge dynamics at various settler's depths when subjected to shock loads is shown in the top diagram of Figure 5. Feed concentration was deliberately increased from 5,260 g/m^3 to 8,000 g/m^3 at the second hour followed by reduction to 2000 g/m^3 at the 15th hour. The effect of shock loads appears to be most significant at the settler depth of 1.25 m, which is the feed location and it is gradually reduced at other positions as the fluid moves either upward or downward. These shock loads do not appear to affect the sludge dynamics at the upper zone with depth 0.1 m, which is largely due to the fact that the original "steady-state" concentration is already very low. At the bottom of the settler with depth

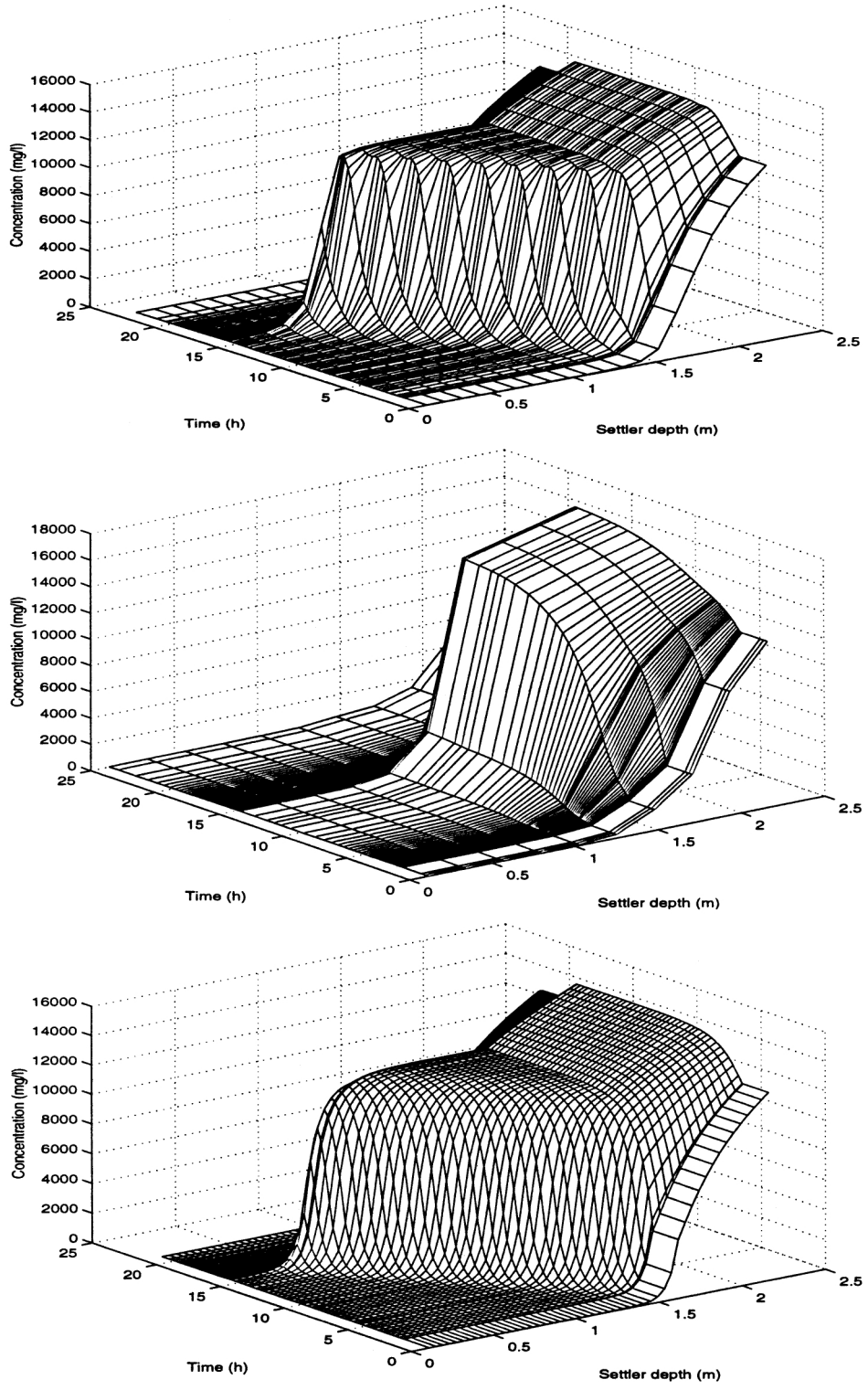

Figure 5. 3-D plots of sludge dynamics (20 layers (top figure), 10 layers (middle figure), 50 layers (bottom figure)).

2.16 m, sludge dynamics is still pronounced. This means that at a given high shock load as used in the example simulation, the returned activated sludge will certainly affect the performance of the activated sludge reactor if they are not controlled at an early stage. The surface plot of the simulated sludge dynamics with the 20-layer, double-Peclet model appears to be reasonably closed to the surface plot of the more accurate 50-layered model, while the surface plot of the 10-layered model is clearly distorted at the clarification section, particularly below 1.5-m depth. This means that numerical errors are suppressed as the number of layers is increased and the 20-layer double-Peclet settler model is considered

good enough. In fact, integration of the 20-layer settler model into a biological-nutrient-removal activated-sludge process model will result in a large number of ordinary differential equations and hence computation time.

Despite having two additional parameters (total of 7), the computation time required for dynamic simulation by the 20-layer, Takacs' model was two times less than the 20-layer, double-Peclet model. This is largely attributable to the flux-constraining term in the latter. The 20-layer, single-Peclet model, on the other hand, requires 20% less computing time relative to the double-Peclet model, but simulation results are less accurate. The Hamilton model with 20 layers requires the lowest computing time (37% less than the 20-layer, double-Peclet model), which is largely due to the relatively small number of parameters involved, but this model is not recommended for practical use, since it cannot predict the clarification section satisfactorily. Judging from the results of the steady-state validation and the dynamic simulation of the activated-sludge settler, we therefore concluded that the 20-layer, double-Peclet model is the most suitable for integration into the BNR-activated-sludge process model.

Validation of the BNR-activated-sludge process model

The computational algorithm developed in this study will now be applied to model an existing continuous pilot-scale BNR-activated-sludge plant at the Liverpool Sewerage Treatment plant in Sydney, Australia.

Outline of Pilot-Plant Experimental Design and Models Validation. The pilot-plant processes a constant flow of 70 to 90 L/h of screened, degritted sewerage with about 1,000 L capacity in the main bioreactors. The plant setup is essentially similar to Figure 1. Sewerage used in this study was municipal wastewater, sourced from a full-scale wastewater treatment plant located at the same site. The average influent wastewater characteristics and process design parameters used for all simulations are given in Table 6. A total of three RTD, nine pseudo-steady-state and dynamic step-test experiments were conducted to validate the model presented in this article. Validation of the distributed parameter BNR-activated-sludge model proceeded in five stages:

Stage 1. Wastewater characterization to determine average influence concentration of components of interest.

Stage 2. RTD studies, in order to characterize tank hydraulics.

Stage 3. Steady-state and dynamic step-test experiments.

Stage 4. Application of the numerical algorithm to perform steady-state simulation for parameter identification and calibration using experimental data and simulation results.

Stage 5. Application of the numerical algorithm and the results of stages 1 to 4 to simulate dynamics of components within the anaerobic, anoxic, and aerobic zones, under different perturbation conditions, and test their validity against dynamic experimental results.

Systems Characterization

1. Wastewater Characterization. COD fractionation for components of interest is as follows:

- Fermentation products, considered to be acetate (S_A), were estimated from measurement of the individual acids: acetic, propionic, butyric, and valeric.
- Fermentable, readily biodegradable organic substrates (S_F) were calculated from estimated biodegradable soluble COD (SCOD) and S_A. The estimated biodegradable SCOD is assumed to be the measured SCOD less the estimated soluble inerts, taken to be effluent SCOD measurement.
- Biomass in the influent was not characterized, but the fractions are needed in order to explain the bloom and the washout of certain groups of microorganisms (Henze et al., 1994). Heterotrophic organisms (X_H) and inert particulates (X_I) are assumed to be 15 and 10% of the measured total COD, respectively, which are within the recommended range (Henze, 1992; Henze et al., 1994; and Johannsson, 1994). Two other biomass groups in the influent wastewater required in this study, autotrophs (X_{AUT}) and PAO (PAO is further divided into three distinct particulate groups: X_{PAO}, X_{PHA}, and X_{PP}) in most cases are believed to be very small (Henze et al., 1994) and are therefore assigned small values on the order of 0–1 mg COD/L.
- Slowly biodegradable substrate (X_S) in the influent is calculated by subtracting all COD-contributing components from total COD.

Characterization of nutrients unlike COD or biomass is rather straightforward, since the components of interest, that is, ammonia-nitrogen (S_{NH_4}), soluble phosphate (S_{PO_4}) assumed to be orthophosphate, and oxidized nitrogen (S_{NO_x}), were measured using standard laboratory methods (Greenberg et al., 1985).

2. Bioreactors Hydraulic Characterization. RTD experimental design: one-shot rhodamine tracer was independently introduced into the inlet of the anaerobic, anoxic, and aerobic zones. Grab samples were collected at the outlet of each zone for 2, 1.5, and 3.5 h at intervals of 5, 5, and 10 min, respectively. Samples were than analyzed for tracer's concen-

Table 6. Basic Data for Process Simulation

Parameters	Value	Units
Influent wastewater characteristics		
Dissolved oxygen, S_{O_2}	0	$mg_{O_2}L^{-1}$
Nitrate, S_{NO_3}	0.1	$mg_N L^{-1}$
Ammonia, S_{NH_4}	37.6	$mg_N L^{-1}$
Alkalinity, S_{ALK}	5	$mole_{HCO_3^-}L^{-1}$
Acetate, S_A	140	$mg_{COD}L^{-1}$
Fermentable readily biodegradable COD, S_F	58	$mg_{COD}L^{-1}$
Phosphate, S_{PO_4}	8.1	$mg_P L^{-1}$
Nitrifying organisms, X_{AUT}	2.99	$mg_N L^{-1}$
Heterotrophs, X_H	89.7	$mg_{COD}L^{-1}$
Slowly biodegradable COD, X_S	185.38	$mg_{COD}L^{-1}$
Phosphorus-accumulating organisms, X_{PAO}	1	$mg_P L^{-1}$
Poly-hydroxy alkanoate, X_{PHA}	1	$mg_N L^{-1}$
Poly-phosphate, X_{PP}	0.5	$mg_P L^{-1}$
Design parameters		
Anaerobic reactor volume	148	m^3
Anoxic reactor volume	186	m^3
Aerobic reactor volume	658	m^3
RAS tank volume	204	m^3
Normal influent flow	70.1	$L \cdot d^{-1}$
Normal RAS flow	61.8	$L \cdot d^{-1}$
Normal internal recycle flow	192.5	$L \cdot d^{-1}$
Settler depth	2.5	m
Settler cross-sectional area	0.78754	m^2
Peclet number (anaerobic)	3.5	
Peclet number (anoxic)	1.0	
Peclet number (aerobic)	2.5	

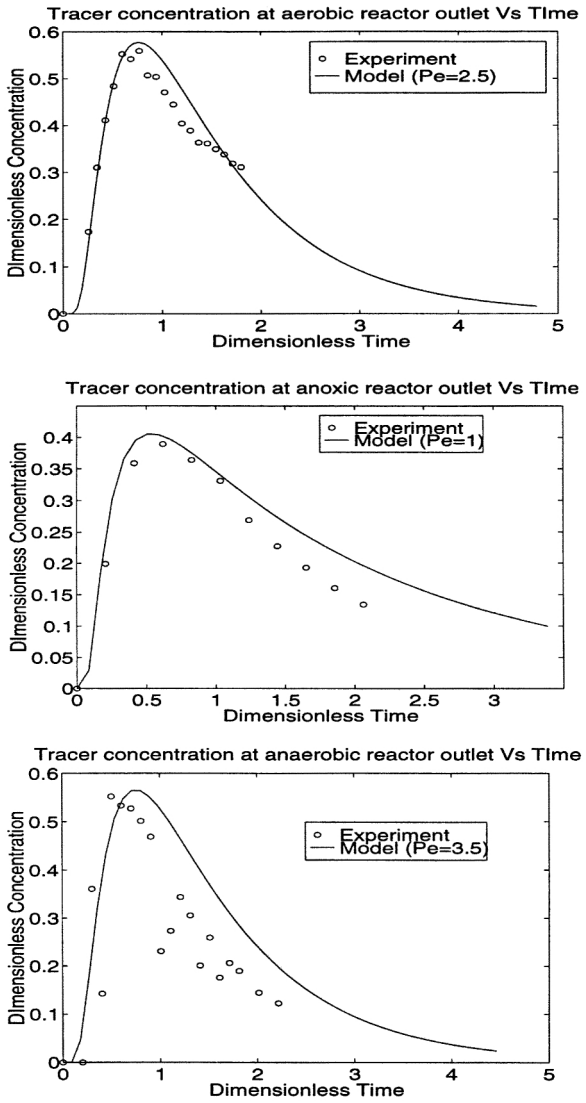

Figure 6. Tracer concentration at the outlet of aerobic (top figure), anoxic (middle figure), and anaerobic (bottom figure) zone using the correlation of Levenspiel and Smith (1957).

tration. The dimensionless tracer's concentration at the outlet of each zone can be approximated by the following expression (Levenspiel and Smith, 1957):

$$C_\theta = \frac{1}{2\sqrt{\pi\tau(1/Pe)}} \exp\left(\frac{-(1-\tau)^2}{4\tau(1/Pe)}\right), \qquad (15)$$

where τ = dimensionless time.

Figure 6 shows the results of RTD studies in this work. The aerobic zone is considered to be well fitted for an axial dispersion model with a Peclet number of 2.5. On the other hand, simulated results for the anoxic and the anaerobic zones give slower tails or are rather poorly fitted at the "second half" of the RTD experimental curve. This is attributable to the fact that recycled tracer was not accounted for in Eq. 15, and furthermore, some difficulties were encountered in collecting samples at the outlet of the anaerobic zone, which is in fact the first compartment of the anoxic zone. On the other hand, fitting of the models with Peclet numbers of 1 and 3.5 to the "first half" of the RTD curves, the rise time, is considered to be fair. This is largely because the tracer had not yet recycled during this period. Since the evaluated Peclet numbers of the bioreactors are not considered to be too large for this process (Arceivala, 1981; Lee et al., 1999a), five collocation points should be sufficiently accurate for simulation with the orthogonal collocation technique.

Steady-State Calibration of Model Parameters

1. Steady-State Experimental Design. Prior to conducting dynamic step-test experiments, grab samples of the wastewater at various locations within the Sydney Wastewater pilot plant were collected for analysis of pseudo-steady-state conditions. The data of interests were (1) total suspended solids (X_{TSS}); (2) total COD; (3) soluble COD (SCOD); (4) ammonia nitrogen (S_{NH_4}); (5) nitrate and nitrite (oxidized) nitrogen (S_{NO_x}); (6) soluble phosphate (S_{PO_4}); (7) dissolved oxygen (S_{O_2}); (8) oxygen uptake rate (OUR). These pseudo-steady-state data will then be used for parameter identification and model calibration.

2. Procedure for Calibration. There are 57 parameters related to the kinetics of biological nitrogen and phosphorus removal in the model, which are listed in Table 1. With this many parameters, it is difficult, if not impossible, to calibrate them together to fit the simulated results against the experimental data. Henze et al. (1994) suggested a somewhat loose but practical idea to calibrate the ASM No. 2 kinetic model. Two of their key suggestions adopted in this work follow:

1. Most parameters should not be changed during calibration, since they do not vary significantly from case to case. Nine kinetic parameters considered as constants (see Table 1) are: Y_H, Y_{AUT}, μ_H, $K_{O_2\_het}$, K_F, K_{A_het}, K_{NO_3}, $K_{O_2\_aut}$, and $K_{NH_4\_aut}$.
2. Nonsensitive parameters should not be changed. In fact, if changes are made to these parameters in an illogical direction and rely solely on fitting the experimental data, the model may be distorted too far from reality, which is a dangerous precedent.

A self-explanatory procedure used in this work for calibration of the BNR-activated-sludge model is given as follows:

1. Obtain initial values of kinetic and settling parameters.
2. Perform steady-state simulation.
3. Perform sensitivity analysis to identify parameters for calibration. Nonsensitive parameters should be left unchanged.
4. Do parameter estimation. This can be done manually and/or using nonlinear programming tools such as the NIMBUS (Newell and Cameron, 1990) prototype optimizer [based on FSQP, an optimization package of Zhou and Tits (1993)], to try to fit simulated results to an experimental data set such that the sum of the square errors (SSE) of the measured and simulated values of variables of interest is minimized. Due to the highly interactive nature of some of the parameters and the limited number of parameters that can be handled at a time, only key stream properties such as concentration of S_{PO_4} and S_A at the outlet of the anaerobic zone, S_{PO_4}, S_{NO_3}, and S_{NH_4} at the outlet of anoxic or aerobic zones should be fitted. Constraints imposed on the parameters to be estimated should be within a "reasonable" range. As an example q_{PP}

(the rate constant for aerobic storage of X_{PP}) should not be adjusted too high such that X_{PP} is larger than X_H, which is unrealistic (Choi and Lee, 1996) when optimizing S_{PO_4} within the aerobic zone.

5. Check the errors of simulated results with experimental data. When the optimizer is used, errors may be unacceptably high due to unconverged results of the optimizer hitting the constraint(s). Redefine constraint(s) on the affected parameter(s) and repeat step number 4.

3. Parameter Sensitivity. A systematic way of quantifying variables' sensitivity to a parameter is simply by perturbing the parameter, resimulating, and calculating the so-called normalized sensitivity factor (NSF). NSF is given by

$$\mathrm{NSF}_i = \frac{\dfrac{\partial S_i}{S_i}}{\dfrac{\partial \theta_j}{\theta_j}} \approx \frac{\dfrac{\Delta S_i}{S_i}}{\dfrac{\Delta \theta_j}{\theta_j}}. \qquad (16)$$

A large NSF_i indicates that parameter θ_j is sensitive to variable S_i and vice versa. Results from this parameter sensitivity study, detailed in Lee (1998), shows that q_{PHA} (rate constant for storage of X_{PHA}) is much more sensitive to S_A, S_{PO_4}, S_{NO_3}, X_{PAO}, and X_{PHA} than other components at the outlet of anaerobic, anoxic, and aerobic zones. On the other hand, calculated NSF for $K_{NH_4\_he}$ (saturation coefficient for ammonium) and i_{PSF} (phosphate content of soluble substrate) were generally much smaller than q_{PHA}, and therefore these are considered insensitive to the process and should be considered constant. Other IAWQ kinetic parameters found sensitive to the stream data are q_{DNP} (rate constant for denitrifying PAO) b_{pp} (rate constant for lysis of X_{PP}), K_{max} (maximum ratio of X_{PP}/X_{PAO}), $\eta_{NO_3\_he}$ (anoxic hydrolysis reduction factor), q_{fe} (maximum rate for fermentation), and K_{A_pa} (saturation coefficient for S_A).

Parameters related to PAO such as q_{PHA} and q_{DNP} considered to be highly uncertain and/or sensitive to process variables were optimized such that simulated steady-state results are as close as possible to experimental data, achieving the lowest possible SSE. For simulation with the double-Peclet settler model, settling parameters are calibrated to try to fit simulated values with experimental total suspended solids (X_{TSS}) in the effluent and the RAS flow. In most of the cases q_{PHA} had to be increased to try to improve fitting of S_A and S_{PO_4} in the anaerobic zone. The rate constant for phosphorus uptake in the anoxic zone (q_{DNP}) needs to be smaller than the aerobic zone (q_{PP}) in order to improve the fitting of S_{PO_4} in the anoxic and the aerobic zones, respectively. The parameter q_{DNP} is also found to be effective for fitting S_{NO_3} within the anoxic zone. This is as expected, since S_{NO_3} is one of the limiting components appearing in the rate equation for anoxic storage of X_{PP} (see Table 2). Such biological phosphorus uptake calibration nevertheless seems to be risky at the moment, since it may vary from place to place. For the base-case simulation, fitting of experimental X_{TSS} in the RAS line is largely dictated by the Vesilind's settling parameter, V_O and the Peclet numbers to a lesser degree. Pe_{bot} and Pe_{up} were used as "fine"-fitting parameters after "rough" treatment of the experimental X_{TSS} with V_O.

In order to obtain a reasonably good fit of the nitrate profile in the anoxic zone, our simulation experience suggested that η_{NO_3} should at least be kept identical to the default literature value if not reduced, thus contradicting the suggestion by Henze et al. (1994). This anomaly can be explained by the insignificant effect of the anoxic growth of heterotrophic bacteria, X_H, on denitrification. In fact, adjusting the q_{DNP} parameter is found to be more appropriate, since all state variables in the rate equation for anoxic storage of X_{PP} are "active," while some of the state variables in the rate equation for anoxic growth of X_H (that is, S_A and S_F) are zero or close to zero when the partially treated wastewater reaches the anoxic zone. Other IAWQ parameters were kept identical to the values suggested by Henze et al. (1994) since they are either reasonably stable or process variables are insensitive to parameter perturbations. Generally the final optimized IAWQ kinetic parameters for all nine experiments were all within the same order of magnitude as that given by Henze et al. (1994), and the settling parameters were practically the same for each experiment. The 11 identified parameters (q_{PHA}, q_{PP}, q_{DNP}, b_{pp}, K_{max}, $\eta_{NO_3\_he}$, q_{fe}, K_{A_pa}, Pe_{bot}, Pe_{up}, V_O) with values given in Tables 1 and 5 are thus considered realistic.

Examples of Steady-State Calibration Results. Figure 7 (top) shows the steady-state profile of simulated SCOD compared

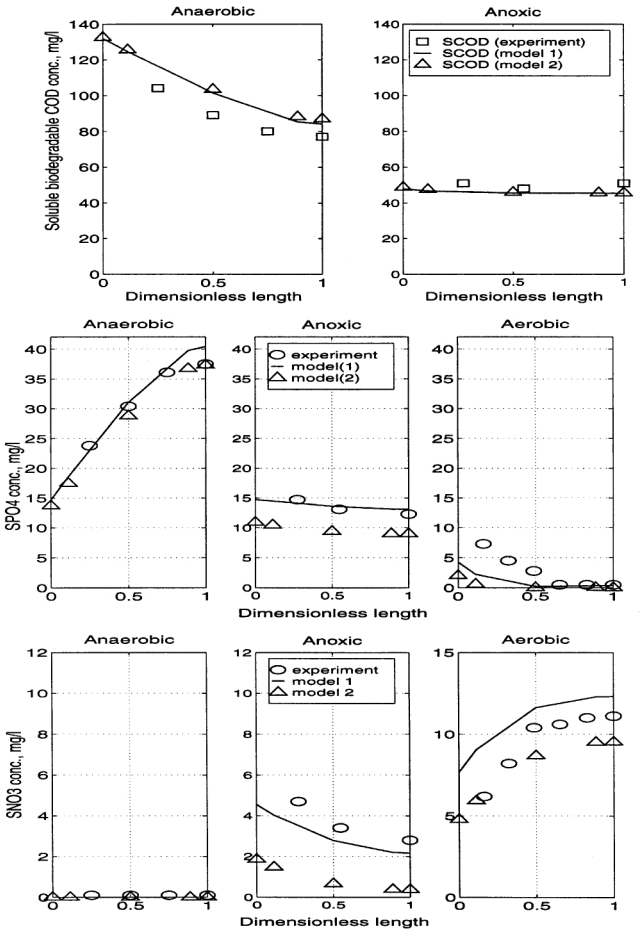

Figure 7. Steady-state profiles of SCOD (top figure), S_{PO_4} (middle figure) and S_{NO_3} (bottom figure).

with the experimentally determined filtered COD for the aerobic and the anaerobic zones. Model 1 uses the double-Peclet settler model, whereas model 2 uses the simple settler scheme described by Olsson and Andrews (1978). Since the experimental data points do not correspond directly to the three internal collocation points, the exact locations of the former are normalized to dimensionless length. The gradient of the SCOD with respect to reactor length within the anaerobic zone appears to be rather sharp, indicating a high removal rate of readily biodegradable COD (represented by fermentable, readily biodegradable COD (S_F), and fermentation products (S_A) in the model). Referring to the reduced-order kinetic for the anaerobic zone (see Table 2), S_F is typically converted to S_A by the heterotrophic organisms (X_H), while S_A is consumed by PAO during the anaerobic stage. The rather flat SCOD profile within the anoxic zone indicates that it largely contains soluble unbiodegradable COD. This means that most if not all of S_F and S_A are virtually depleted on entering the anoxic zone.

The fate of S_{PO_4} and S_{NO_3} at various zones are shown in Figure 7 (middle and bottom). Evidently, there is a net reduction of these nutrients within the anoxic zone as expected, since the modified kinetic model of the ASM No. 2 allows for denitrification by PAO, at the expense of PHA. The simulated profile of S_{NO_3} within this zone with Model 1 is much better than Model 2, largely because of the flexibility of changing the multiparameter double-Peclet settler model (model 1), compared with the single-parameter settler model (model 2). Difficulty arises in improving profiles of S_{NO_3} further and S_{PO_4} to a lesser extent due to the high coupling of the processes within the different zones. Our simulation experience indicated that small changes to the value of parameters such as q_{PP} and q_{PHA} affects the simulated results considerably. Simulated S_{NO_3} profiles within the aerobic zone are nevertheless reasonably close to the experimental data in both cases.

Validation of Bioreactor Dynamics: Anaerobic Zone

1. Experimental Design. Three dynamic step-test experiments (A, B, and C) were conducted within this zone. For experiment A, the influent flow was stepped up from 70.7 L/h to 140 L/h for 90 min, followed by stepping down to its original flow. Other flow rates for the experiment were RAS flow = 44 L/h; NO_x recycle flow = 195 L/h. For experiment B, a step change on the RAS flow from 44 L/h to 98 L/h was performed for 90 min, before stepping down to its original flow. Other flow rates for the experiments were influent flow = 70.7 L/h; NO_x recycle flow = 195 L/h. For experiment C, S_A in the influent wastewater was stepped from 107 mg COD/L to 307 mg COD/L by introducing the external acid dosage for 90 min. Flow rates for the experiments were influent flow = 70.7 L/h; NO_x recycle flow = 195 L/h; and RAS flow = 70.7 L/h. For all experiments, grab samples were collected at the outlet of the second compartment within the anaerobic zone every 10 min for 200 min. Samples were analyzed for S_A and S_{PO_4}.

2. Results and Discussion. The sampling point for the anaerobic zone step tests was at the middle of the 4-compartment anaerobic reactor, which corresponds exactly to collocation point number 3 of the numerical algorithm. Dynamic simulations were performed on the entire plant, although only the anaerobic zone was investigated. Simulated results compared with data from experiment A are shown in Figure 8. Evidently the dynamics of acetate and soluble phosphate are well predicted by the two models. The components' dynamic behavior is as expected, since an increase in influent flow rate means that the HRT within the system drops. Consequently, the rates of acetate uptake and soluble phosphate released by PAO are reduced. It is also expected that concentration of all other particulates will also be reduced due to the decreased residence time.

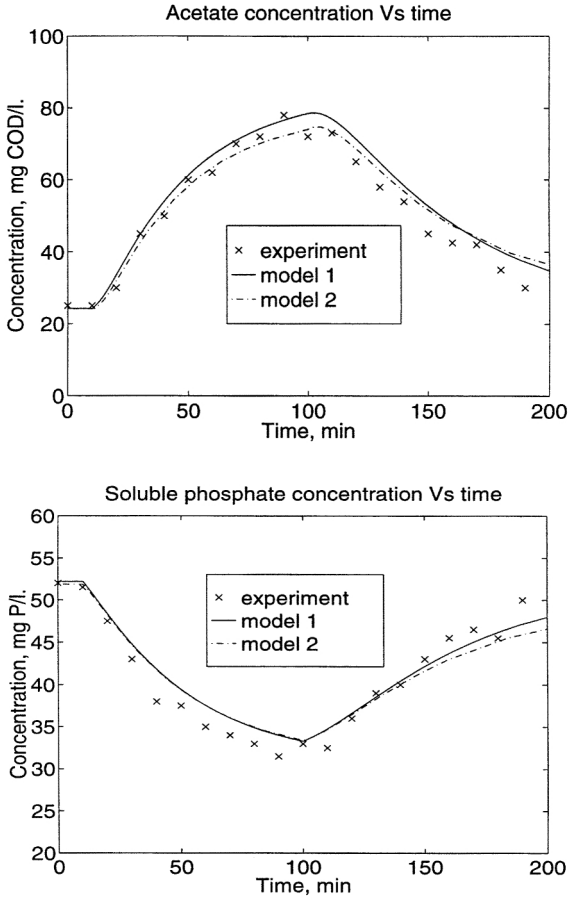

Figure 8. Dynamics of S_A (top figure) and S_{PO_4} (bottom figure) at the anaerobic zone's second compartment outlet under perturbations on the influent flow (experiment A).

The effects of disturbance in the influent S_A (experiment B) on the dynamics of S_A within the anaerobic zone are shown in Figure 9 (top). Experimental observation deviates significantly from theoretical predictions by either of the models. It appears that the rate at which S_A is consumed by PAO for storage in the PHA may well be higher than expected. One other biological reason is the presence of the so-called G-bacteria (Cech et al., 1993; Cech and Hartman, 1993; Smolders et al., 1995), a group of bacteria that are able to take up S_A under anaerobic conditions but do not remove phosphorus. This group of bacteria, not accounted for in the model, may have contributed to the additional S_A uptake seen in the experimental data. Nevertheless, further increasing the value of parameter q_{PHA}, rate constant for PHA storage, can easily circumvent the plant-model mismatch. We ruled out changes

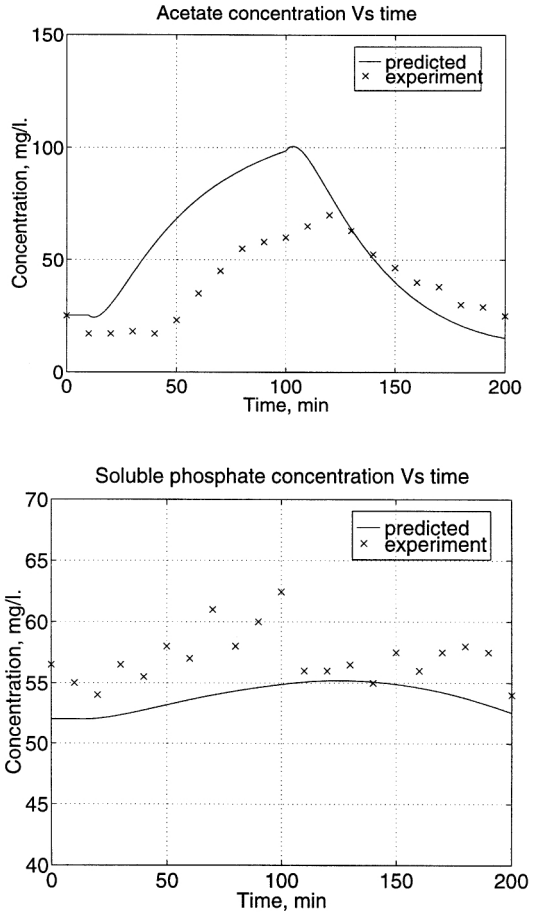

Figure 9. Dynamics of S_A (top figure) and S_{PO_4} (bottom figure) at the anaerobic zone's second compartment outlet under perturbations on the influent S_A (experiment B).

in the flow patterns within the anaerobic zone as the reason for the lag time of more than 20 min in the S_A dynamics since the perturbation point is so close to the sampling point (collocation point number 3). Experimental errors during sample collection may have been the reason for such mismatch. On the other hand, predicted dynamics of acetate during step-down stage are reasonable.

The fate of soluble phosphate is shown in Figure 9 (bottom). As with acetate, the predicted dynamics of soluble phosphate is not as good as expected during stepping up of influent acetate concentration. These results suggest that the large differences in the predicted dynamics and experimental data may be due to experimental errors, particularly during sample collection, apart from the expected plant− model mismatch. The zigzag pattern in the experimental data points of the soluble phosphate dynamics can be attributable to measurement errors. As far as the behavior of the two species under investigation is concerned, their dynamics are qualitatively correct. Stepping up of influent acetate means that more acetate is available in the system, to be taken up by PAO with a corresponding release of soluble phosphate. It is expected that during this period, there will be a net increase in the biomass concentrations, except for poly-phosphate.

The effects of step changes to RAS flow (experiment C) on soluble phosphate dynamics is shown in Figure 10. Predicted results from Model 2 are considered reasonably good and slightly better than Model 1. This observation is particularly true during stepping up of the RAS flow. The behavior of soluble phophate is as expected, since stepping up the RAS flow means that more biomass exists in the system, that is, there is a net increase in the biomass concentration. Alteration to the system hydraulics results in a net reduction in the soluble materials' concentration, including soluble phosphate. The results from this dynamics simulation study suggested that the benefits of employing the more sophisticated double-Peclet settler model as opposed to the simple settler model are insignificant, as far as prediction of species dynamics within the bioreactors is concerned. This means that the latter, which is essentially a reduced-order model of the former, should be good enough for simulation of the BNR-activated-sludge process.

Anoxic Zone

1. Experimental Design. As with the anaerobic zone, three dynamics step-test experiments (D, E, and F) were conducted within this zone. In experiment D, the NO_x recycle flow was changed twice from 180 L/h to 300 L/h, and then to 50 L/h before returning to the origin. The duration of each of the two step disturbances was 60 min. Other flow rates for the experiment were influent flow = 65.7 L/h; RAS flow = 90 L/h. In experiment E, the RAS flow was changed twice from 90 L/h to 147 L/h, and then to 43 L/h before returning to the origin. The duration of each of the two step disturbances was 60 min. Other flow rates for the experiments were influent flow = 72.5 L/h; NO_x recycle flow = 190 L/h. In experiment F, S_{NO_x} concentration in the NO_x recycle line was stepped up by 10.3 mg N/L using a solution of sodium nitrate for 60 min. Actual flow rates for the experiment were influent flow = 69.7 L/h; RAS flow = 84 L/h; and NO_x recycle flow = 191 L/h. For all experiments, grab samples were taken from the end of the anoxic zone every 15 min for 4 h. Samples were analyzed for S_{NO_x} and S_{PO_4}.

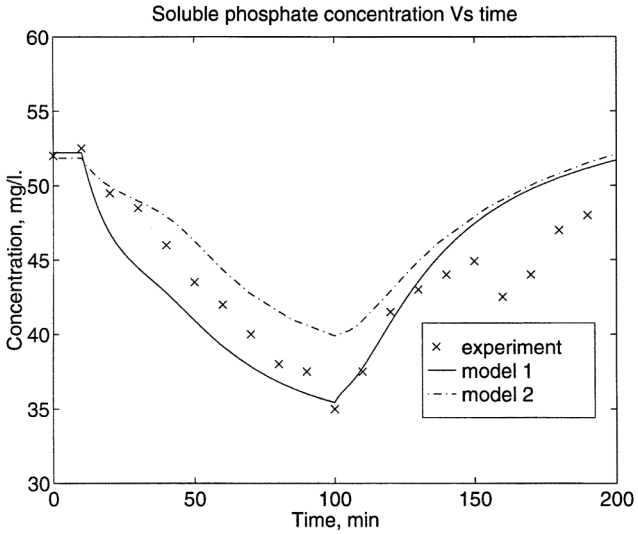

Figure 10. Dynamics of S_{PO_4} at the anaerobic zone's second compartment outlet under perturbations on RAS flow (experiment C).

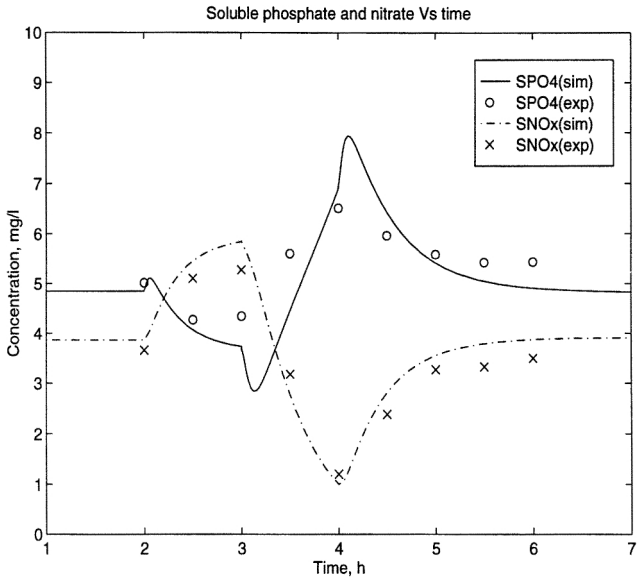

Figure 11. Dynamics of S_{PO_4} and S_{NO_x} at outlet of the anoxic zone under perturbations on NO_x recycle flow (experiment D).

2. Results and Discussion. Figures 11 to 13 show simulated results against plant data for experiments D to F, respectively. It can be seen that the model predicts S_{NO_x} dynamics quite well and S_{PO_4} to an acceptable degree. These good results are attributable in part to the inclusion of the kinetic of denitrifying PAO within the anoxic zone, which is largely thought to be responsible for phosphorus uptake (P-uptake) by utilizing S_{NO_x} as the electron acceptor in the absence of oxygen. The rate of P-uptake within this zone is relatively slower than the aerobic zone, as indicated by the smaller values of the rate constant, q_{DNP}, compared with q_{PP} in all the experiments investigated (see Table 1).

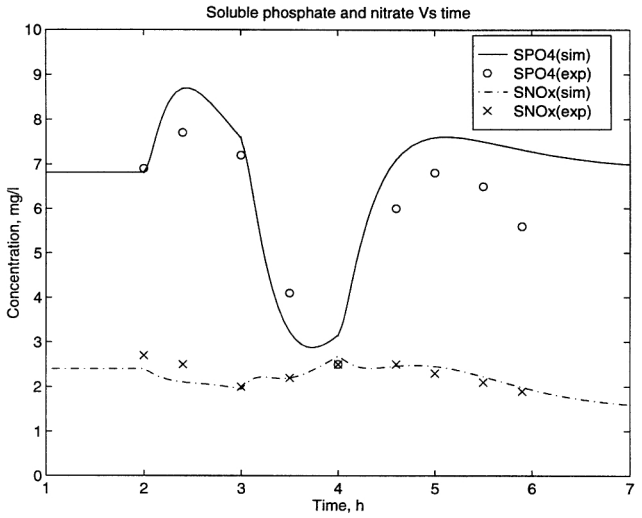

Figure 12. Dynamics of S_{PO_4} and S_{NO_x} at outlet of the anoxic zone under perturbations on RAS flow (experiment E).

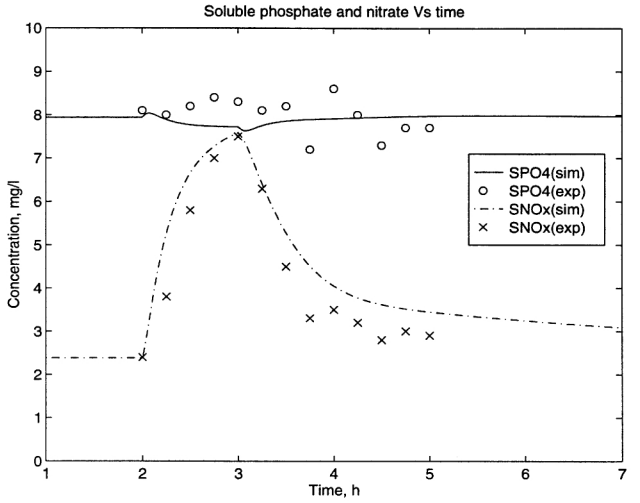

Figure 13. Dynamics of S_{PO_4} and S_{NO_x} at outlet of the anoxic zone under external-NO_x spike (experiment F).

In Figure 11, the dynamics behavior of S_{PO_4} and S_{NO_x} are as expected, since an increase in the NO_x recycle flow means that more S_{NO_x} is available in the system, which could then be used by the denitrifying PAO to take up additional S_{PO_4}. In Figure 12, an initial increase in S_{PO_4} may be attributable to an increase in the lysis of X_{PP}. An increase in the RAS flow in this case means that more biomass is present in the system. As a result of this, the growth of autotrophic bacteria (X_{AUT}) in the aerobic zone is adversely affected, less ammonia (S_{NH_4}) is converted to S_{NO_x}, and therefore the S_{NO_x} recycled to the anoxic zone is reduced. In Figure 13, the S_{NO_x} spike at the inlet of the anoxic zone has a similar effect on S_{NO_x} and S_{PO_4} dynamics as in experiment D (perturbation to NO_x recycle flow). The rate of S_{PO_4} reduction from the second hour to the third hour was nevertheless marginally lower in this experiment. The experimental data of S_{PO_4} appears to be scattered, especially between the third hour and the fourth hour, which was probably due to outliers.

Aerobic Zone

1. Experimental Design. As with the anaerobic and anoxic zones, three dynamic step-test experiments (G, H, and I) were conducted within this zone. In experiment G, DO setpoints within the aeration compartment one of the aerobic zone were adjusted hourly for 4 h from (1) to (4): (1) 2–3 mg/L; (2) 4–5 mg/L; (3) 1–2 mg/L; (4) 0.5–1 mg/L; (5) 2–3 mg/L. Actual flow rates for the experiment were influent flow = 70.2 L/h; RAS flow = 85.3 L/h; and NO_x recycle flow = 178 L/h. Since the outlet of compartment one of the six-compartment aerobic zone falls between collocation 2 and 3, we must obtain an average setpoint of the DO steps and do an interpolation for model simulation. A single, PI control loop is then formed around the first compartment to facilitate DO setpoint steps. In experiment H, the RAS flow was changed twice from 81.8 L/h to 128.3 L/h, and then to 30 L/h before returning to the origin. The duration of each of the two step disturbances was 60 min. Other flow rates for the experiments were influent flow = 75.1 L/h; RAS flow = 84.7 L/h. In experiment I, ammonia in the first compartment of the aerobic zone was

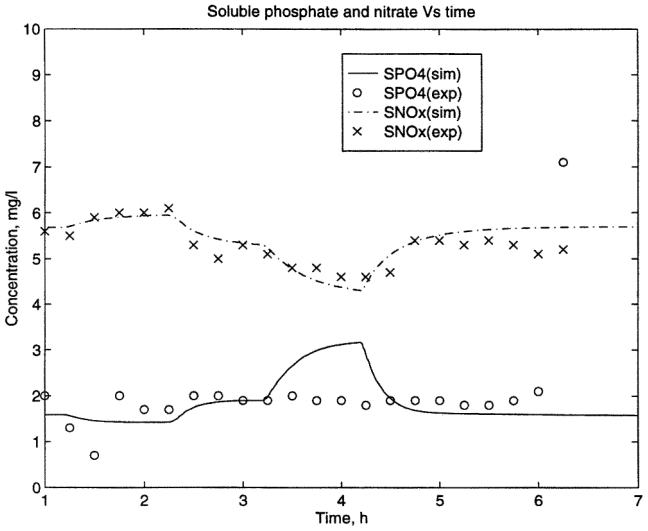

Figure 14. Dynamics of S_{PO_4} and S_{NO_x} within the first compartment of the aerobic zone under perturbations on DO setpoint (experiment G).

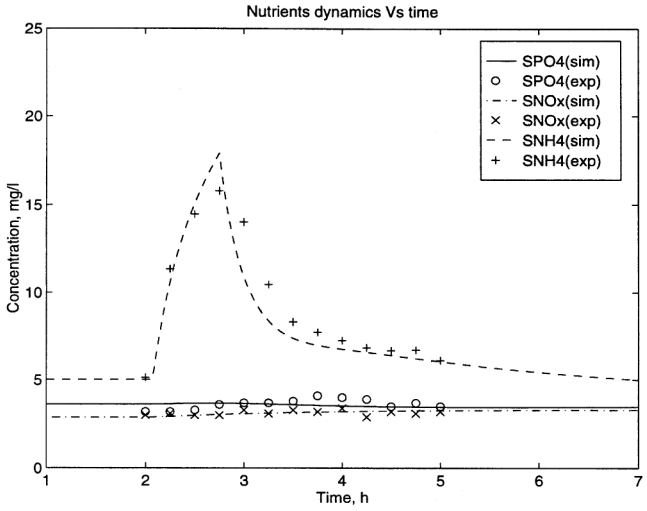

Figure 16. Dynamics of S_{PO_4}, S_{NO_x} within the first compartment of the aerobic zone under S_{NH_4} spike (experiment I).

stepped up by 15.4 mg N/L using a solution of ammonium chloride for 45 min. Actual flow rates for the experiments were influent flow = 75.1 L/h; NO_x recycle flow = 181 L/h; RAS flow = 84.7 L/h. For all experiments, grab samples were taken from the same compartment every 15 min for 5 h. Samples were analyzed for S_{NO_x} and S_{PO_4}.

2. Results and Discussion. Figures 14 to 16 show simulated results against plant data within the first compartment of the aerobic zone for experiments G to I, respectively. In all the cases investigated, S_{NO_x} dynamics is considered to be well predicted. Simulated S_{PO_4} in experiment G deviates significantly from the experimental data, particularly between the third and the fourth hour (see Figure 14) when the DO setpoint was dropped. This may, however, just require reduction in the value of q_{PP}, the rate constant for aerobic storage of X_{PP}. Between the first and the second hour, simulated S_{PO_4} does drop when the DO setpoint was increased, but the second and the third experimental data points are much lower, thus suggesting that the model does not capture this response adequately. Further research to investigate the relationship between DO and S_{PO_4} is necessary. Figure 14 also shows that nitrification still occurred even though the DO setpoint was stepped down after the second hour. This result is attributable to the relatively slower dynamics of S_{NO_x} compared with DO.

The behavior of S_{PO_4} and S_{NO_x} in experiment H (Figure 15) is as expected. An increase in the RAS flow from the second to the third hour means that more biomass is available in the system, but due to lack of nutrients, the rate of lysis of X_{AUT} increased, causing a reduction in S_{NO_x} and hence a rise in S_{NH_4} (plant data not available for validation). Similarly, an increase in the rate of lysis of X_{PP} causes an increase in S_{PO_4} in the system. In Figure 16, changes in the dynamics of S_{PO_4} is deemed too small to allow a fair comparison of plant data and model prediction. Had a large S_{NH_4} spike been employed, a better comparison of results would have resulted.

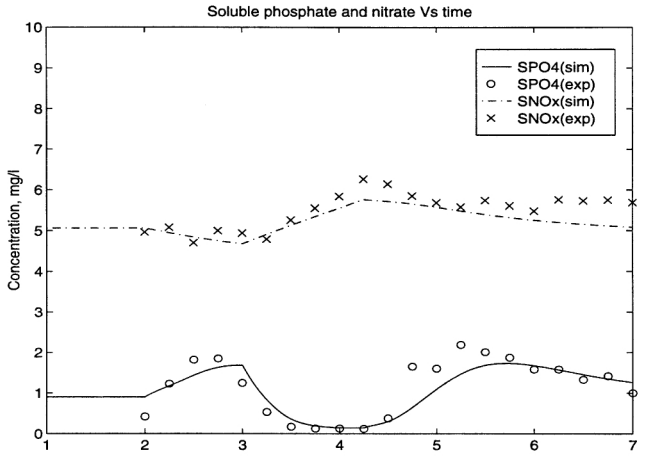

Figure 15. Dynamics of S_{PO_4} and S_{NO_x} within the first compartment of the aerobic zone under perturbations on RAS flow (experiment H).

Conclusions and Recommendations

The following can be concluded from this study:

- A distributed-parameter model that addresses the hydraulics of the main bioreactors of the BNR-activated-sludge process has been formulated in this article. Using the distributed-parameter BNR-activated-sludge bioreactor model and the orthogonal collocation numerical technique, a new computational algorithm has been developed for the simulation of single-sludge, continuous plants treating nutrients (phosphorus and nitrogen) from municipal wastewater. The utility of this computational algorithm has been demonstrated in this article by a comprehensive validation study on an existing pilot plant.
- The results of steady-state fitting of highly uncertain and/or sensitive IAWQ kinetics and settling parameters with nine sets of independently acquired plant data show that val-

ues of the kinetic parameters were within the same order of magnitude as in the literature, while the settling parameters were practically the same for each experiment and therefore considered to be realistic.

- Based on a total of nine sets of experimentally designed dynamics step-tests, model prediction of the dynamics of components within the three different bioreaction zones is found to be generally good, with the exception of S_A in the anaerobic zone and S_{PO_4} in the aerobic zone in two experiments.
- Distributed-parameter modeling of the activated-sludge secondary settler was addressed in this article. The proposed 20-layer, double-Peclet settler model outperformed other state-of-the-art settler models investigated in this study. Simulation results of this model with different operating conditions showed that it can predict the full-scale experimental data reasonably well.
- The benefits of employing a sophisticated settler model such as the state-of-the-art layered model is insignificant as far as simulation of the BNR-activated-sludge bioreactors is concerned.

The following topics are recommended for further study:

- Prediction of the S_A dynamics in the anaerobic zone can be improved by including a model of G-bacteria, a newly identified group of bacteria (by others), and the associated glycogen storage into the reduced-order kinetic models. In the case of S_{PO_4} dynamics, further research is necessary to ascertain the relationship between DO and S_{PO_4} dynamics. The fact that there are still a number of microbiological and biochemical aspects of the BNR-activated-sludge process yet to be addressed in the existing kinetic models (Ekama and Wentzel, 1997) could have also contributed to the plant–model mismatch found in this work. As it is, the computational algorithm may, despite the apparent deficiencies, be a useful tool not only for prediction of process behavior but also for control purposes and possible design assistance, provided it is used judiciously.
- To reflect the reality of full-scale plants, verification and validation of the model, following diurnal variation of influent flows and the concentration of components of interest, should be conducted, before using it for the design of new plants or improving the operation and control of full-scale plants.
- One particular area deliberately omitted in this study is checking the mass balances of COD, nitrogen, and phosphorus, which if done properly may improve confidence of the plant data used for steady-state parameter estimation. One reason for this omission is that the phenomenon of COD loss in the BNR-activated-sludge system is yet to be resolved, as pointed out by Barker and Dold (1995, 1997b). The kinetic model used in this work only assumes COD loss via fermentation, sequestration, and hydrolysis under anoxic/anaerobic, which is still questionable.
- Since the characterized bioreactor hydraulic models have different Peclet numbers, it could be valuable to investigate the difference between the distributed parameter (or PDE) approach and the standard tanks-in-series technique for the BNR-activated-sludge system. This future work will require characterization of the bioreactor hydraulics using the standard tanks-in-series technique, new computer codes for process simulation, and model calibration.

Acknowledgment

The data used for BNR-activated sludge model simulation in this work was made possible by a collaborative research and development project between the University of Queensland and industrial partners. This is gratefully acknowledged. We are indebted to all members in the Novel Process Control for Wastewater Treatment for providing these valuable data without which this article would not have been completed.

Literature Cited

Ante, A., H. U. Besche, and H. Voss, "A Mathematical Model for Enhanced Biological Phosphorus Removal," *Water Sci. Tech.*, **30**, 193 (1994).

Arceivala, S. J., *Wastewater Treatment and Disposal*, Dekker, New York (1981).

Barker, P. S., and P. L. Dold, "Denitrification Behaviour in Biological Excess Phosphorus Removal Activated Sludge Systems," *Water Res.*, **30**, 769 (1996).

Barker, P. S., and P. L. Dold, "General Model for Biological Nutrient Removal Activated Sludge Systems: Model Presentation," *Water Environ. Res.*, **69**, 969 (1977a).

Barker, P. S., and P. L. Dold, "General Model for Biological Nutrient Removal Activated Sludge Systems: Model Application," *Water Environ. Res.*, **69**, 985 (1977b).

Cech, J. S., P. Hartman, and J. Wanner, "Competition Between PolyP and Non-PolyP Bacteria in an Enhanced Phosphate Removal System," *Water Environ. Res.*, **65**, 690 (1993).

Cech, J. S., and P. Hartman, "Competition Between Polyphosphate and Polysaccharide Accumulating Bacteria in Enhanced Biological Phosphate Removal System," *Water Res.*, **27**, 1219 (1993).

Choi, E. S., and H. S. Lee, "Biological Nutrient Removal Characteristics of Low Strength Municipal Wastewater," *Korean J. Chem. Eng.*, **13**, 364 (1996).

Coe, H. S., and G. H. Clevenger, "Methods for Determining the Capacities of Slime-Settling Tanks," *Trans. AIME*, **55**, 356 (1916).

Danckwerts, P. V., "Continuous Flow Systems, Distributions of Residence Times," *Chem. Eng. Sci.*, **2**, 1 (1953).

Ekama, G. A., and M. C. Wentzel, "Difficulties and Development in Biological Nutrient Removal Technology and Modelling," *Proc. BNR3 Conf. Biological Nutrient Removal, IAWQ/AWWA*, Brisbane, Australia, p. 3 (1997).

Greenberg, A. E., R. R. Trussell, and L. S. Clesceri, eds., *Standard Methods for the Examination of Water and Wastewater*, 16th ed., American Public Health Association (APHA) (1985).

Grijsperdt, K., P. Vanrolleghem, and W. Verstraete, "Selection of One Dimensional Sedimentation Models for On-line Use," *Water Sci. Tech.*, **31**, 193 (1995).

Hamilton, J., R. Jain, P. Antoniou, S. A. Svoronos, B. Koopman, and G. Lyberatos, "Modelling and Pilot-Scale Experimental Verification for Predenitrification Process," *J. Environ. Eng.*, **118**, 38 (1992).

Hartel, L., and H. J. Popel, "A Dynamic Secondary Clarifier Model Including Processes of Sludge Thickening," *Water Sci. Tech.*, **25**, 267 (1992).

Henze, M., "Characterization of Wastewater for Modelling of Activated Sludge Processes," *Water Sci. Tech.*, **25**, 1 (1992).

Henze, M., C. P. L. Grady, W. Gujer, G. R. van Marais, and T. Matsuo, "Activated Sludge Model No. 1," IAWPRC Sci. Tech. Rep. No. 1, IAWPRC, London (1987).

Henze, M., W. Gujer, T. Mino, T. Matsuo, M. C. Wentzel, and G. R. van Marais, "Activated Sludge Model No. 2," IAWQ Sci. Tech. Rep. No. 2, IAWQ, London (1994).

Jeppsson, U., and S. Diehl, "An Evaluation of a Dynamic Model of the Secondary Clarifier," *Proc. Water Quality. Int. '96, IAWQ 18th Biennial Int. Conf.*, Singapore (1996).

Johannsson, P., "SIPHOR: A Kinetic Model for Simulation of Biological Phosphate Removal," PhD Diss., Lund University, Lund, Sweden (1994).

Koehne, M., K. Hoen, and M. Schuhen, "Modelling and Simulation of Final Clarifiers in Wastewater Treatment Plants," *Math. Comp. Sim.*, **39**, 609 (1995).

Kynch, G. J., "A Theory of Sedimentation," *Trans. Faraday Soc.*, **48**, 166 (1952).

Lee, T. T., "Distributed Parameter Modelling and Advanced Control Strategies Applied to the Activated Sludge Process," PhD Thesis, The Univ. of Queensland, Brisbane, Australia (1998).
Lee, T. T., F. Y. Wang, and R. B. Newell, "On the Evaluation of the Exit Boundary Condition of a Cyclic Bioreactor System Using the Axial Dispersion Theory," *Chem. Eng. Tech.*, **21**, 901 (1998).
Lee, T. T., F. Y. Wang, and R. B. Newell, "Dynamic Modelling and Simulation of Activated Sludge Process Using Orthogonal Collocation Approach," *Water Res.*, **33**(1), 73 (1999a).
Lee, T. T., F. Y. Wang, and R. B. Newell, "Dynamic Simulation of Activated Sludge Process Using Orthogonal Collocation on Finite Element," *Comput. Chem. Eng.* (1999b).
Levenspiel, O., *Chemical Reaction Engineering*, Wiley, New York (1972).
Levenspiel, O., and W. K. Smith, "Notes on the Diffusion-Type Model for the Longitudinal Mixing of Fluids in Flow," *Chem. Eng. Sci.*, **6**, 227 (1957).
Newell, R. B., and I. T. Cameron, *NIMBUS Users Manual*, Computer-Aided Process Engineering Centre, Dept. of Chemical Engineering, The Univ. of Queensland, Brisbane, Australia (1991).
Olsson, G., and J. F. Andrews, "The Dissolved Oxygen Profile—A Valuable Tool for Control of the Activated Sludge Process," *Water Res.*, **12**, 985 (1978).
Olsson, G., and R. B. Newell, *Wastewater Treatment Systems: Modelling, Diagnosis and Control*, IWA Publishing, London (1999).
Otterpohl, R., and M. Freund, "Dynamic Models for Clarifiers of Activated Sludge Plants with Dry and Wet Weather Flows," *Water Sci. Tech.*, **26**(5–6), 1391 (1992).
Pflanz, P., "Performance of (Activated Sludge) Secondary Sedimentation Basins," *Advances in Water Pollution Research*, S. H. Jenkins, ed., *Proc. Int. Conf.*, Prague, p. 21 and 569 (1969).
Reklaitis, G. V., A. Ravindran, and K. M. Ragsdell, *Engineering Optimization: Methods and Applications*, Wiley, New York (1983).
Sen, D., and C. W. Randall, "General Activated Sludge Model for Biological Nitrogen and Excess Phosphorus Removal," *Design and Retrofit of Wastewater Treatment Plants for Biological Nutrient Removal*, C. W. Randall, J. L. Banard, and H. D. Stensel, eds., Technomic, Lancaster (1992).
Smolders, G. J. F., J. van der Meij, M. C. M. van Loosdrecth, and J. J. Heijnen, "A Structured Metabolic Model for Anaerobic and Aerobic Stoichiometry and Kinetics of the Biological Phosphorus Removal Process," *Biotech. Bioeng.*, **47**, 277 (1995).
Takacs, I., G. G. Patry, and D. Nolasco, "A Dynamic Model of the Clarification-Thickening Process," *Water Res.*, **25**, 1263 (1991).
Vesilind, P. A., "Design of Prototype Thickener from Batch Settling Tests," *Water Sewage Works*, **115**, 302 (1968).
Villadsen, J., and M. L. Michelsen, *Solution of Differential Equation Models by Polynomial Approximation*, Prentice-Hall, Englewood Cliffs, NJ (1978).
Vitasovic, Z. Z., "Continuous Settler Operation: Dynamic Model," *Dynamic Modelling and Expert System in Wastewater Engineering*, G. G. Patry and D. Chapman, eds., Lewis, Chelsea, MI, p. 59 (1989).
Wachtmeister, A., T. Kuba, M. C. M. Van Loosdrecht, and J. J. Heijnen, "A Sludge Characterization Assay for Aerobic and Denitrifying Phosphorus Removing Sludge," *Water Res.*, **31**, 471 (1997).
Watts, R. W., S. A. Svoronos, and B. Koopman, "One-Dimensional Modeling of Secondary Clarifiers Using a Concentration and Feed Velocity-Dependent Dispersion Coefficient," *Water Res.*, **30**, 2112 (1996).
WRC, "Theory, Design and Operation of Nutrient Removal Activated Sludge Processes," Water Research Commission, Pretoria, South Africa (1984).
Zhou, J. L., and A. L. Tits, "Nonmonotone Line Search for Minimax Problems," *J. Opt. Theory and Appl.*, **76**(3), 455 (1993).

Appendix

Discretization of the main bioreactor using orthogonal collocation

Based on a detailed numerical study on the distributed parameter bioreactor model by Lee et al. (1999b), it was concluded that selection of an appropriate numerical technique depends largely on the system's moving front, which is characterized by the Peclet number. Although good numerical properties such as accuracy, low computing time, and numerical stability are desirable, these may not be achievable due to factors such as limitation on the number of discretization allowed in a particular software. If the Peclet number of either the anaerobic, anoxic, or aerobic zones of the BNR-activated-sludge process is small, that is, in the neighborhood of 1, the orthogonal collocation technique should first be attempted, since it requires a low number of discretization while maintaining high accuracy. Readers interested in the details of the analysis of the numerical methods applied to continuous activated-sludge bioreactor systems should refer to Lee et al. (1999b) or Lee (1998). Applying collocation to Eq. 1, the generalized model-collocation for the main bioreactors of the BNR-activated-sludge process is given by

$$\frac{dC_{k,j}}{dt} = \frac{1}{\mathrm{HRT}} \cdot \left(\frac{1}{Pe} \sum_{i=1}^{N+2} B_{j,i} \cdot C_{k,i} - \sum_{i=1}^{N+2} A_{j,i} \cdot C_{k,i} \right) + \sum_{p=1}^{NP} \upsilon_{p,k}\, \rho_{p,j} + M_{k,j}, \quad \text{(A1)}$$

where j = the collocation number; N = the number of inernal collocation points; and A and B are the orthogonal collocation matrices for the first- and second-order derivatives, respectively. The collocation models for Eqs. 2 to 4 are therefore given by Eqs. A2 to A4:

$$\frac{dS_{\mathrm{A},j}}{dt} = \frac{1}{\mathrm{HRT}} \cdot \left(\frac{1}{Pe} \sum_{i=1}^{N+2} B_{j,i} \cdot S_{\mathrm{A},i} - \sum_{i=1}^{N+2} A_{j,i} \cdot S_{\mathrm{A},i} \right) + r_{\mathrm{ferm},j} - r_{\mathrm{PHA},j} + b_{\mathrm{PHA}} \frac{S_{\mathrm{ALK},j}}{K_{\mathrm{ALK},pa} + S_{\mathrm{ALK},j}} X_{\mathrm{PHA},j}, \quad \text{(A2)}$$

where

$$r_{\mathrm{ferm},j} = q_{fe} \frac{S_{\mathrm{F},j}}{K_{fe} + S_{\mathrm{F},j}} \frac{S_{\mathrm{ALK},j}}{K_{\mathrm{ALK},he} + S_{\mathrm{ALK},j}} X_{\mathrm{PAO},j}$$

and

$$r_{\mathrm{PHA},j} = q_{\mathrm{PHA}} \frac{S_{\mathrm{A},j}}{K_{\mathrm{A}} + S_{\mathrm{A},j}} \frac{S_{\mathrm{ALK},j}}{K_{\mathrm{ALK}} + S_{\mathrm{ALK},j}} \times \frac{X_{\mathrm{PP},j}/X_{\mathrm{PAO},j}}{K_{\mathrm{PP}} + X_{\mathrm{PP},j}/X_{\mathrm{PAO},j}} X_{\mathrm{PAO},j}.$$

$$\frac{dS_{\mathrm{NO_3},j}}{dt} = \frac{1}{\mathrm{HRT}} \cdot \left(\frac{1}{Pe} \sum_{i=1}^{N+2} B_{j,i} \cdot S_{\mathrm{NO_3},i} - \sum_{i=1}^{N+2} A_{j,i} \cdot S_{\mathrm{NO_3},i} \right) - (\mu_{\mathrm{H,anox\_S_F},j} + \mu_{\mathrm{H,anox\_S_A},j}) - r_{\mathrm{pp,store},j} - \frac{(1 - Y_{\mathrm{PAO}})}{2.86 Y_{\mathrm{PAO}}} \mu_{\mathrm{PAO},j}, \quad \text{(A3)}$$

where

$$\mu_{\mathrm{H,anox\_S_F},j} = \hat{\mu}_{\mathrm{H}}\eta_{\mathrm{NO_3},he}\frac{S_{\mathrm{F},j}}{K_{\mathrm{F}}+S_{\mathrm{F},j}}\frac{S_{\mathrm{F},j}}{S_{\mathrm{F},j}+S_{\mathrm{A},j}} \times \frac{S_{\mathrm{NH_4},j}}{K_{\mathrm{NH_4},he}+S_{\mathrm{NH_4},j}}\frac{S_{\mathrm{NO_3},j}}{K_{\mathrm{NO_3},he}+S_{\mathrm{NO_3},j}}\frac{S_{\mathrm{PO_4},j}}{K_{\mathrm{P},he}+S_{\mathrm{PO_4},j}}X_{\mathrm{H},j}$$

$$\mu_{\mathrm{H,anox\_S_A},j} = \hat{\mu}_{\mathrm{H}}\eta_{\mathrm{NO_3},he}\frac{S_{\mathrm{A},j}}{K_{\mathrm{A},he}+S_{\mathrm{A},j}}\frac{S_{\mathrm{A},j}}{S_{\mathrm{F},j}+S_{\mathrm{A},j}} \times \frac{S_{\mathrm{NH_4},j}}{K_{\mathrm{NH_4},he}+S_{\mathrm{NH_4},j}}\frac{S_{\mathrm{NO_3},j}}{K_{\mathrm{NO_3},he}+S_{\mathrm{NO_3},j}}\frac{S_{\mathrm{PO_4},j}}{K_{\mathrm{P},he}+S_{\mathrm{PO_4},j}}X_{\mathrm{H},j}$$

$$r_{\mathrm{pp,store},j} = -\frac{Y_{\mathrm{PHA}}}{2.86}q_{\mathrm{DNP}}\frac{S_{\mathrm{PO_4},j}}{K_{\mathrm{P},pp}+S_{\mathrm{PO_4},j}} \times \frac{X_{\mathrm{PHA},j}/X_{\mathrm{PAO},j}}{X_{\mathrm{PHA},j}+X_{\mathrm{PHA},j}/X_{\mathrm{PAO},j}} \times \frac{K_{\max}-X_{\mathrm{PP},j}/X_{\mathrm{PAO},j}}{K_{\mathrm{IPP}}+K_{\max}-X_{\mathrm{PP},j}/X_{\mathrm{PAO},j}}X_{\mathrm{PAO},j}$$

$$\mu_{\mathrm{PAO},j} = \hat{\mu}_{\mathrm{PAO}}\frac{S_{\mathrm{NO_3},j}}{S_{\mathrm{NO_3},j}+K_{\mathrm{O}}}\frac{S_{\mathrm{NH_4},j}}{S_{\mathrm{NH_4},j}+K_{\mathrm{NH_4}}}\frac{S_{\mathrm{PO_4},j}}{S_{\mathrm{PO_4},j}+K_{\mathrm{P}}} \times \frac{S_{\mathrm{ALK},j}}{S_{\mathrm{ALK},j}+K_{\mathrm{ALK}}}\frac{X_{\mathrm{PHA},j}/X_{\mathrm{PAO},j}}{X_{\mathrm{PHA},j}+X_{\mathrm{PHA},j}/X_{\mathrm{PAO},j}}X_{\mathrm{PAO},j}.$$

$$\frac{dS_{\mathrm{O_2},j}}{dt} = \frac{1}{\mathrm{HRT}}\cdot\left(\frac{1}{Pe}\sum_{i=1}^{N+2}B_{j,i}\cdot S_{\mathrm{O_2},i} - \sum_{i=1}^{N+2}A_{j,i}\cdot S_{\mathrm{O_2},i}\right) + \left(1-\frac{1}{Y_{\mathrm{H}}}\right)(\mu_{\mathrm{H},ae\_S_F,j}-\mu_{\mathrm{H},ae\_S_A,j}) - r_{\mathrm{PHA,store},j} + \left(1-\frac{1}{Y_{\mathrm{PAO}}}\right)\mu_{\mathrm{PAO},j} + \left(1-\frac{4.57}{Y_{\mathrm{AUT}}}\right)\mu_{\mathrm{AUT},j} + Kla\left(S_{\mathrm{O_2\_SAT}}-S_{\mathrm{O_2},j}\right), \quad \text{(A4)}$$

where

$$\mu_{\mathrm{H},ae-S_F,j} = \hat{\mu}_{\mathrm{H}}\frac{S_{\mathrm{O_2},j}}{K_{\mathrm{O_2},he}+S_{\mathrm{O_2},j}}\frac{S_{\mathrm{F},j}}{K_{\mathrm{F}}+S_{\mathrm{F},j}}\frac{S_{\mathrm{F},j}}{S_{\mathrm{F},j}+S_{\mathrm{A},j}} \times \frac{S_{\mathrm{NH_4},j}}{K_{\mathrm{NH_4},he}+S_{\mathrm{NH_4},j}}\frac{S_{\mathrm{PO_4},j}}{K_{\mathrm{P},he}+S_{\mathrm{PO_4},j}}\frac{S_{\mathrm{ALK},j}}{K_{\mathrm{ALK},he}+S_{\mathrm{ALK},j}}X_{\mathrm{H},j}$$

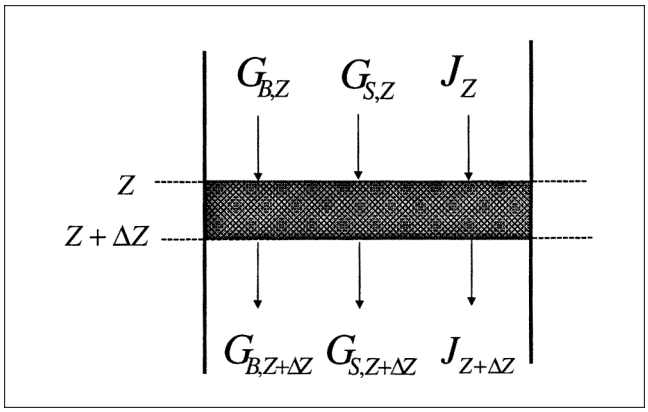

Figure A1. Mass balance at thickening zone.

$$\mu_{\mathrm{H},ae-S_A,j} = \hat{\mu}_{\mathrm{H}}\frac{S_{\mathrm{O_2},j}}{K_{\mathrm{O_2},he}+S_{\mathrm{O_2},j}}\frac{S_{\mathrm{A},j}}{K_{\mathrm{A},he}+S_{\mathrm{A},j}}\frac{S_{\mathrm{A},j}}{S_{\mathrm{F},j}+S_{\mathrm{A},j}} \times \frac{S_{\mathrm{NH_4},j}}{K_{\mathrm{NH_4},he}+S_{\mathrm{NH_4},j}}\frac{S_{\mathrm{PO_4},j}}{K_{\mathrm{P},he}+S_{\mathrm{PO_4},j}}X_{\mathrm{H},j}$$

$$\mu_{\mathrm{PAO},ae,j} = \hat{\mu}_{\mathrm{PAO}}\frac{S_{\mathrm{O_2},j}}{K_{\mathrm{O_2},pa}+S_{\mathrm{O_2},j}}\frac{S_{\mathrm{NH_4},j}}{K_{\mathrm{NH_4},pa}+S_{\mathrm{NH_4},j}} \times \frac{S_{\mathrm{PO_4},j}}{K_{\mathrm{P},pa}+S_{\mathrm{PO_4},j}}\frac{S_{\mathrm{ALK},j}}{K_{\mathrm{ALK},pa}+S_{\mathrm{ALK},j}} \times \frac{X_{\mathrm{PHA},j}/X_{\mathrm{PAO},j}}{X_{\mathrm{PHA},j}+X_{\mathrm{PHA},j}/X_{\mathrm{PAO},j}}X_{\mathrm{PAO},j}$$

$$\mu_{\mathrm{AUT},j} = \hat{\mu}_{\mathrm{AUT}}\frac{S_{\mathrm{O_2},j}}{K_{\mathrm{O_2}}+S_{\mathrm{O_2},j}}\frac{S_{\mathrm{NH_4},j}}{K_{\mathrm{NH_4}}+S_{\mathrm{NH_4},j}} \times \frac{S_{\mathrm{PO_4},j}}{K_{\mathrm{P}}+S_{\mathrm{PO_4},j}}\frac{S_{\mathrm{ALK},j}}{K_{\mathrm{ALK}}+S_{\mathrm{ALK},j}}X_{\mathrm{AUT},j}.$$

Similar equations can be developed for other components in the BNR-activated-sludge model for anerobic, anoxic, and aerobic zones using the generalized collocation model of the BNR-activated-sludge process. For low Peclet numbers, these discretized model equations are solved together with the discretized Danckwerts boundary conditions for the inlet and exit of the bioreactor given by the general Eqs. A5 and A6, respectively:

$$C_1 = \frac{A_{N+2,N+2}\left(\sum_{i=2}^{N+1}A_{1,i}\cdot C_i + Pe\cdot C_a\right) - A_{1,N+2}\sum_{i=2}^{N+1}A_{N+2,i}\cdot C_i}{A_{1,N+2}A_{N+2,1} - A_{N+2,N+2}\cdot(A_{1,1}-Pe)} \quad \text{(A5)}$$

$$C_{N+2} = \frac{\left(\frac{1}{Pe}A_{1,1}-1\right)\sum_{i=2}^{N+1}A_{N+2,i}\cdot C_i - A_{N+2,1}\left(\frac{1}{Pe}\sum_{i=2}^{N+1}A_{1,i}\cdot C_i + C_a\right)}{\frac{1}{Pe}A_{N+2,1}A_{1,N+2} - \left(\frac{1}{Pe}\cdot A_{1,1}-1\right)A_{N+2,N+2}}. \quad \text{(A6)}$$

It should be pointed out that even if we apply three internal collocation points ($N = 3$) to each of the species of interest within the three main bioreactors, a complete computer algorithm that includes a 20-layer double-Peclet settler model, lumped parameter models of the deoxic zone, and RAS tank, as well as equations that represent the two mixing streams and two splitting streams shown in Figure 1, would result in 156 ODE and 328 algebraic!

Derivation of the distributed-parameter settler model

Figure A1 shows the individual components of solids fluxes, that is, gravity-settling flux (G_s) and bulk flow (G_b) within the thickening zone. To account for the nonideality of flow, or in other words, fluid flow is not true plug flow, which is evident in this unit operation (WRC, 1984), reduction in the total solids flux due to back mixing is included (that is, the dispersive flux, J, in Figure A1).

Assuming a constant volume for a given layer, ΔZ, and making a mass balance at a very thin section with a length of ΔZ, we have

$$A \cdot \Delta Z \cdot \frac{\partial X}{\partial t} = A \cdot G_B|_Z - A \cdot G_B|_{Z+\Delta Z} + A \cdot G_S|_Z - A \cdot G_S|_{Z+\Delta Z} + A \cdot J|_Z - A \cdot J|_{Z+\Delta Z}, \quad \text{(A7)}$$

where A = the cross-sectional area of the settling tank, and X is solids concentration. The dispersive flux, J, is defined as

$$J = -D_S \frac{\partial X}{\partial Z}, \quad \text{(A8)}$$

where D_S is a dispersion coefficient of sludge. Inserting Eq. A8 into Eq. A7 and rearranging, we have

$$\frac{\partial X}{\partial t} = \frac{-A(G_B|_{Z+\Delta Z} - A \cdot G_B|_Z)}{A \cdot \Delta Z} - \frac{A(G_S|_{Z+\Delta Z} - G_S|_Z)}{A \cdot \Delta Z} + \frac{A \cdot D_S\left(\left.\frac{\partial X}{\partial Z}\right|_{Z+\Delta Z} - \left.\frac{\partial X}{\partial Z}\right|_Z\right)}{\Delta Z}. \quad \text{(A9)}$$

Taking the limits of ΔZ approaching zero in Eq. A9, we have

$$\frac{\partial X}{\partial t} = -\frac{\partial G_B}{\partial Z} - \frac{\partial G_S}{\partial Z} + \frac{\partial}{\partial Z}\left(D_S \cdot \frac{\partial X}{\partial Z}\right). \quad \text{(A10)}$$

The downward bulk flux and gravity-settling flux in the Eq. A10 are mathematically defined as

$$G_B = \frac{Q_U}{A} X \quad \text{and} \quad G_S = V_S X. \quad \text{(A11)}$$

Inserting Eq. A11 into Eq. A10, and after some algebra, we obtain the model for solids dynamics within the thickening zone given by Eq. 5. The model for solids dynamics within the clarification zone is similarly derived and results in Eq. 7.

Manuscript received Oct. 19, 1998, and revision received June 4, 1999.